Title: Coordinated Postnatal Trajectories of T Cells and Microbiota in Preterm and Full-term Newborns

Authors: Alex Grier[1#], Nathan Laniewski[2#], Ann L. Gill[2], Haeja A. Kessler[2], Heidie Huyck[3], Jeanne Holden-Wiltse[4], Sanjukta Bandyopadhyay[4], Jennifer Carnahan[3], Andrew Dylag[3], David J. Topham[2], Ann R. Falsey[5], Mary T. Caserta[3], Gloria S. Pryhuber[3], Steven R. Gill[2], Andrew McDavid[4†], Kristin M. Scheible[3†*]

Affiliations:

[1]University of Rochester, Genomics Research Center

[2]University of Rochester, Department of Microbiology and Immunology

[3]University of Rochester, Department of Pediatrics

[4]University of Rochester, Department of Biostatistics and Computational Biology

[5]University of Rochester, Department of Medicine

* Corresponding Author: Kristin_Scheible@urmc.rochester.edu

†#Authors contributed equally to this manuscript

One Sentence Summary: Synchronized patterns of development of the immune system and microbiome in pre- and full-term infants are disrupted as a marker of respiratory disease.

Abstract:

With birth, there is a dramatic increase in an infant's T cell exposures to commensal and pathogenic bacteria. We hypothesized that populations of T cells and microbiota co-develop in the human neonate, and that disruption of their coordination would associate with respiratory morbidity in the first year of life. To test this hypothesis, we analyzed blood and microbiota samples from 133 pre- and 79 full-term infants (PT and FT, respectively), collected through the Prematurity, Respiratory, Immune System and Microbiome (PRISM) study through one year of age. T cell function and phenotype were repeatedly measured by flow cytometry over the first year of life and summarized into immune state types (ISTs). Intestinal and nasal microbiota were measured weekly prior to hospital discharge, monthly thereafter, and during symptomatic respiratory illnesses, and were summarized into community state types (CSTs). Our major findings were three-fold. First, PT and FT CSTs and ISTs varied at birth, but showed an organized progression by postmenstrual age, and convergence by one year. Second, temporal associations between CSTs and ISTs suggest a bidirectional relationship between the microbiome and T cell development. Third, respiratory morbidity is increased in the first year of life in infants displaying atypical acquisition and maturation of microbiota and immune cell populations. These results together suggest that microbiota and T cell maturation are coordinated during infant development. Most importantly, atypical or asynchronous microbiota and T cell maturation is a risk factor for respiratory morbidity in the first year of life.

Introduction

Human newborns are highly susceptible to severe illness and chronic respiratory morbidity with frequent viral respiratory infections (1, 2). Additionally, infants born prematurely have up to a 50% risk for recurrent cough and rehospitalization in the first year, most frequently associated with viral infections, and even a portion of healthy-born full-term infants will suffer from similar morbidity (3). Because T cells are critical in clearing viral pathogens and supporting the formation of protective memory, elevated risk in newborns has traditionally been attributed to either immunodeficiency secondary to the immature adaptive immune systems or, alternatively, to injury induced by an exuberant inflammatory response (4). Our recent prospective study of 277 preterm (PT, < 37 0/7 weeks gestation) and full-term FT (>/= 37 0/7 weeks gestation) infants in the Prematurity and Respiratory Outcomes Program (PROP), showed that CD31+ CD4+ T cells, a population enriched for recent thymic emigrants, were protective against chronic respiratory morbidity in infants born prematurely (5, 6). In particular, the persistence of low CD31+ CD4+ T cell frequency in PT infants at approximately 40 weeks postmenstrual age (PMA), suggesting delayed immune maturation, corresponded to higher risk for persistent respiratory disease (PRD) in the first year. We have also reported characteristic development of both the nasal and gut microbiota associated with prematurity, day of life, and PMA (7, 8). Two recent studies demonstrate that the nasopharyngeal microbiome and virome together predict infant respiratory tract infection but fail to take the state of immune development into account (9, 10). Early adaptation or maladaptation of the immune system to early colonizers undoubtedly relates to an infant's risk for respiratory morbidity, but characterizing the relative importance of immune development in the context of microbial exposures individually and synergistically has been elusive.

A growing number of studies hint at a complex, developmentally-determined immune program influenced by early clinical exposures and microbial colonization (11-13). For example, Olin *et al*. recently demonstrated major shifts in the bulk immune cell populations over the first 3 months of life that followed a predictable pattern according to days of life (14). Early gut dysbiosis, indicated by particularly low microbiota diversity, was associated with an altered balance of immune cell populations, though deeper phenotyping of T cells was not reported. We propose that understanding interrelated infant T cell and microbiota developmental trajectories will reveal markers of predisposition to respiratory illness and shape causative models that link early prenatal and postnatal events, including preterm birth and microbiota and immune development, to long-term health outcomes.

The objectives of this current study were to construct a comprehensive model that describes concordant and discordant developmental trajectories of both T cells and the microbiota in the first year; to characterize the relationship between microbiota and T cell variation after adjusting for birth events and gestational age; and, finally, to assess the impact of abnormal T cell-microbiota trajectories on risk for PRD and respiratory infection. Here we report, for the first time, that while the development of T cells and microbiota of the gut and respiratory tract are indeed strongly coupled to PMA, some T cell-microbiota associations exist independently of gestational age at birth and PMA, and atypical or mistimed development of either the microbiome or T cells relative to host age is a marker of respiratory morbidity during infancy.

Results

Study Design and Demographics

Neonatal subjects (n=267) born 23-42 weeks gestational age (GA) were recruited within 7 days of birth at the University of Rochester from 2012-2016, as part of the NIAID-sponsored Prematurity, Respiratory, Immune Systems and Microbiomes study (PRISM) (Fig. 1). In all, 122 preterm (PT, < 37 0/7 weeks gestation) and 80 full-term (FT, ≥ 37 0/7 weeks gestation) subjects completed the study to 12 months of age corrected for premature birth and were categorized as having or not having the primary outcome persistent respiratory disease (PRD) using previously published criteria (15). Among these, 52 PT subjects (43%) and 17 FT subjects (21%) met the criteria for PRD. Sufficient blood to perform T cell phenotyping by flow cytometry was collected from 55% of subjects at birth, 61% of subjects at NICU discharge, and 38% at 12 months. Complete (two staining panels) immunophenotyping for all three timepoints was performed on 25% of subjects, and 63% of subjects had complete immunophenotyping for at least one timepoint. For microbiota profiling, after sample processing, 16S rRNA sequencing, quality control, and removing subjects without any immunophenotyping data, 149 subjects yielded 1748 usable nasal samples and 143 subjects yielded 1899 usable rectal samples. Finally, 109 and 117 subjects had sufficient combined T cell phenotyping and microbiota data to be

included for immunome-nasal microbiota and immunome-rectal microbiota association analyses, respectively (Supplementary Tables 1-2). Cohort demographics are shown in Table 1.

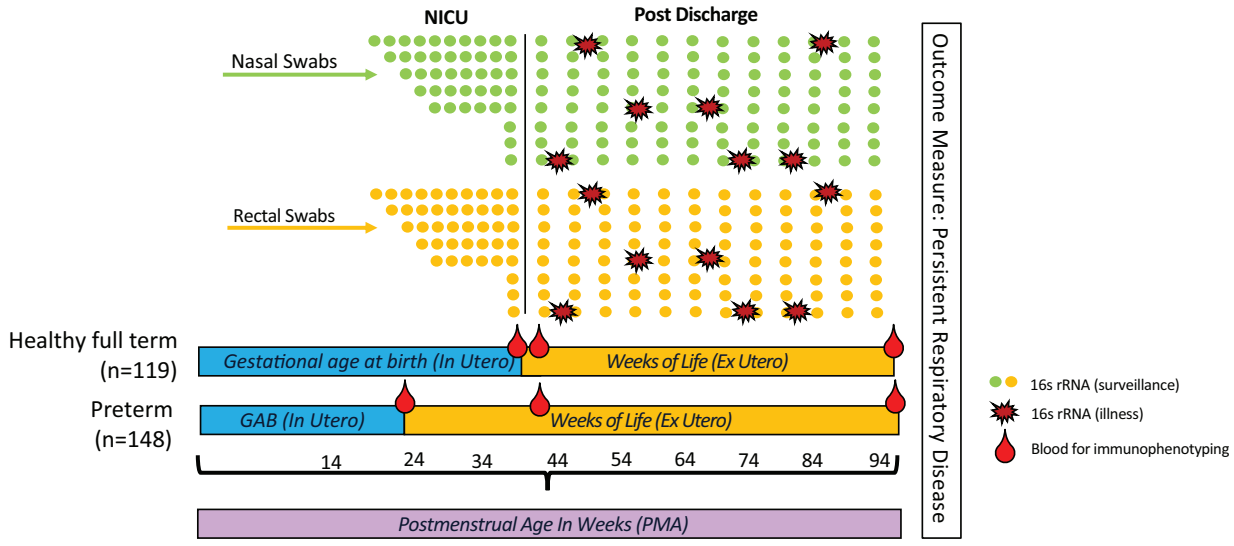

Fig. 1. Study Design. A total of 119 full term and 148 preterm infants were recruited at birth. Swabs were obtained of the nares and rectum to be used for 16S rRNA sequencing (microbiota) weekly in the NICU prior to discharge, monthly post-discharge, and when symptoms of respiratory illness were present. Blood was collected at birth (cord blood), hospital discharge or 36-42 weeks postmenstrual age (whichever was first), and again at 12 months. The 12 month outcome of persistent respiratory disease was determined based on quarterly surveys assessing respiratory morbidity.

	Preterm (n=148)	Term (N=119)
Gestational age (weeks)	29.8 ± 3.7	39.6 ± 1.0
Birthweight (g)	1406.6 ± 620.8	3471.5 ± 511.4
Female	71.0 (48.0%)	49.0 (41.2%)
Black or Asian race	46.0 (31.1%)	29.0 (24.4%)
Public Insurance	81.0 (54.7%)	59.0 (49.6%)
Maternal smoking postnatal	29.0 (19.6%)	15.0 (12.6%)
Delivered by cesarean section	94.0 (63.5%)	49.0 (41.2%)
Chorioamnionitis	7.0 (4.7%)	4.0 (3.4%)
Funisitis*	35.0 (24.3%)	0 (0.0%)
Pre-eclampsia	26.0 (17.6%)	0
Antenatal steriods	121.0 (81.8%)	0
Postnatal steroids	47.0 (31.8%)	10.0 (8.4%)
BPD	25.0 (16.9%)	0
Supplemental O2 (Median FiO2 for first 14 days, IQR)	21.9% (21-27.8)	21% (room air only)
Postnatal infections (% with culture - positive bacteremia)	24.0 (16.2%)	0
Recieved breastmilk (any)	134.0 (90.5%)	92.0 (77.3%)
Number of illness visits/subject (mean +/- SD)	1.2 (1.9)	1.0 (1.8)
Ventilator days (n)	10.0 ± 18.3	0
PRD**	52.0 (42.6%)	17.0 (21.1%)

Table 1: Subject Demographics
*Funisitis calculated on 144 PT and 27 FT subjects (placental pathology available)
**PRD measured in 122 PT and 80 FT

Respiratory and Gut Microbiota Progression by Postmenstrual Age

Respiratory and gut microbiota samples were assessed by 16S rRNA sequencing as previously described (8). Swabs were obtained on study enrollment, at weekly intervals prior to initial hospital discharge, and monthly following hospital discharge through one year of life. Additional samples were collected during acute respiratory illnesses between discharge and one year. Unweighted Unifrac distances between all samples within each body site were computed as a measure of β-diversity and were used to perform principal coordinate analysis (PCoA). The first principal coordinate (PC1) accounted for 10.8% of the total variation seen in the gut microbiota and 12.2% of the total variation in nasal microbiota. Visualization and annotation of these results revealed that for both body sites, overall sample variation reflected subjects' maturity at birth and PMA at sampling (Fig. 2A-2B). Specifically, position along PC1 corresponds to PMA. Samples lower in PC1 tend to be taken prior to 40 weeks PMA, indicating a unique PT microbiota. Over time, subjects progress along PC1 and PT and FT subjects converge, exhibiting equal representation on the right side of axis 1.

To summarize microbiota composition and facilitate subsequent comparative analyses, we partitioned samples from each body site into "community state types" (CSTs) using Dirichlet Multinomial Mixture (DMM) Models (Fig 2C-2D). Each CST represents an archetypal profile of microbiota composition, and samples are assigned to the CST which best explains their observed makeup. Based on model fit and parsimony, 13 CSTs were defined for both respiratory (nCST) and gut microbiota (gCST) and were numbered sequentially (1-13) according to the average PMA at which samples assigned to that CST were collected. Progression from CST 1 to 13 in the gut and the nose strongly associated with PMA (ANOVA , r^2= 0.57 and 0.61, respectively) (Fig. 2E-2F). Both gCST and nCST 1 were predominated by *Staphylococcus*, which was replaced over time with more niche-specific taxa in later CSTs, including

Enterobacteriales and *Clostridiales* in the gut and *Streptococcus* and *Corynebacterium* in the respiratory tract (Fig. 3A-3B). Several early CSTs with the lowest average PMA were predictably enriched for PT samples. An unexpected observation was that several gCSTs and nCSTs collected at later PMA were overrepresented by either PT or FT subjects per a two-tailed binomial test. For example, gCST 9 contained 78% PT samples and was *Tissierellaceae* dominant, *Bifidobacterium* low, whereas 83% of samples in gCST 10 were from FT subjects, and had high abundances of *Bifidobacterium, Veillonella*, and *Prevotella*. The observed FT or PT bias in CSTs suggests that early life events can persistently influence aspects of microbiota development.

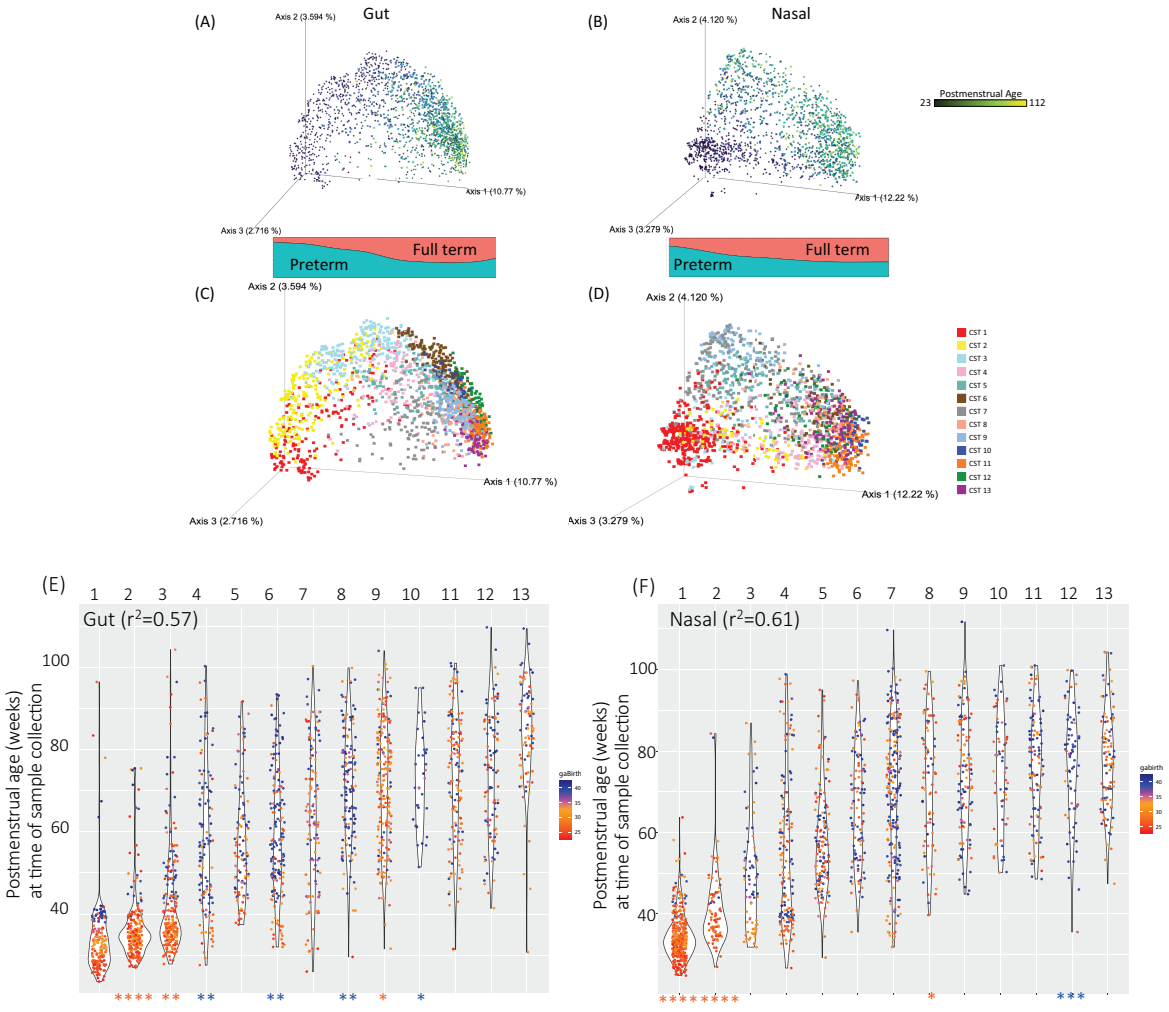

Fig. 2. Progression of microbiota in preterm and full term newborns. Microbiota community profiling was performed on rectal (A, C, E) and nasal (B, D, F) samples obtained from 159 infants during regular surveillance and acute respiratory illness. (A-D) Principal coordinate analysis (PCOA) plots using Unweighted Unifrac distances summarize overall variation and structure. (A-B) Points were colored by postmenstrual age (PMA) at the time the sample was obtained. Colored bands at the base of PCOA plots show the proportion of samples along each point of axis 1 that are from either preterm (teal) or full term (salmon) subjects. (C and D) Microbiota community state types (CST) were defined for each body site, with samples in the PCOA colored according to the CST they represent. CSTs are ordered according to average PMA of occurrence. (E, F) Samples within each CST were plotted against subjects' PMA at the time of sample collection. Each dot represents a single sample, and is colored by the subject's gestational age at birth. R2 values show correlations between CST and PMA. Asterisks at base of dot plots indicate significant enrichment for either preterm (red) or full term samples (blue) (*p<0.05, **p<0.01, ***p<0.001, ****p<0.0001).

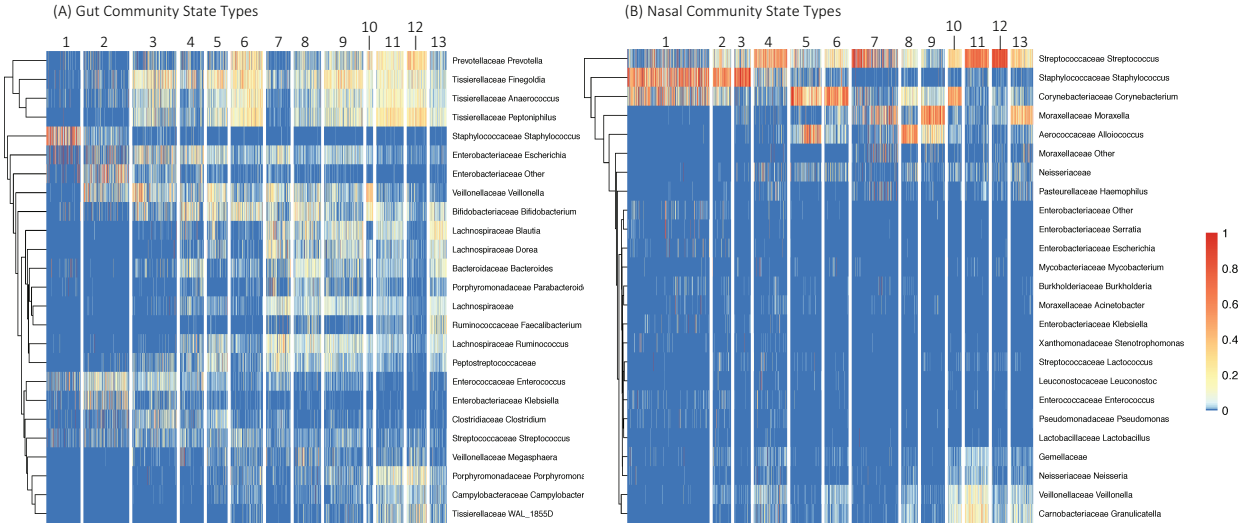

Fig. 3. Microbiota community state type composition. Microbiota community state types (CST) were constructed for each body site and were numbered sequentially based on the average postmenstrual age (PMA) at which they occurred. Composition of each CST based on the 25 most abundant genera overall within each body site is shown in heatmaps (A – gut; B – nose).

T cell development in newborns

We next sought to characterize associations between PMA and T cell phenotype. T cell phenotyping (Tphe) was performed by flow cytometry using blood samples collected at birth, hospital discharge (or 36-42 weeks PMA, whichever came first) and 12 months of gestationally corrected age. Cells were thawed and prepared for staining with a T cell phenotyping panel ("Tphe", total 414 samples). A separate intracellular cytokine antibody panel was also used to stain cells stimulated in vitro with Staphylococcal Enterotoxin B (SEB) ("ICS", total 404 samples) (staining panel details available in Supplementary Fig 1). The clustering algorithm FlowSOM was used to identify unique populations of T cells, or "metaclusters" (Fig 4A) (16), which were grouped according to the following established naming conventions: memory, naive, T follicular helper (TFH), central memory (CM), T regulatory (Treg), naïve recent thymic emigrants (RTE), virtual memory (Vmem), terminal effector (TE), cytotoxic CD8+ (17-22).

To visualize a longitudinal trajectory of T cells, uniform manifold approximation and projection (UMAP) was applied to each sample, without regard to subject-level clinical features. Each sample's Tphe and ICS profiles combined in this case represented a single feature in the UMAP (Fig. 4B), revealing a pattern similar to the microbial progression; PT and FT T cell phenotype and function clustered separately at birth, less so at discharge, and appeared fully convergent by 12 months. Metaclusters that were different between PT and FT subjects were observed almost exclusively at birth and discharge timepoints (Fig. 4D, Supplementary Fig. 2). Many PT-associated populations were Tregs, memory and effectors. Tphe metaclusters enriched in FT were mostly naïve and Vmems with high CD31+ and IL7rα expression. ICS metaclusters enriched in PT were naïve CD45RA+ T cells with either TNFα, IL-2 or no detectable cytokines. FT ICS metacluster cytokine function was characterized by high IL-8 and IL-2.

The majority of metaclusters could serve as simple linear predictors of PMA (Fig. 4C). Both CD4+ and CD8+ T cells displayed a TE phenotype at the earliest PMA, which then transitioned to predominantly naive T cells, followed by CM and then Vmem by one year PMA. The nature and abundance of cytokine functions varied with both GA and PMA. Activated TNFα+, IL-2+ or cytokine null CD4+ and CD8+ metaclusters were higher at the earliest PMA, after which IL-8 became the dominant cytokine. IL-8-positive subpopulations showed minimal TNFα expression, suggesting that these functions may be counter-regulated within the cell. Canonical polarized (CD45RA-, IFNγ, IL-4, IL-17 or CD107a) T cells were frequent only at the 12 month timepoint. The exception to the delayed polarized T cell development was a single IL-4-positive CD8+ metacluster, which was only seen at the youngest PMA. Utilizing the three timepoints typically captured for each subject, we identified 10 metaclusters with non-monotone V- or inverted-V trajectories from birth to 12 months in PT samples (Fig. 4E, Supplementary

Fig. 3). Most frequently, these metacluster abundance followed a V-shaped trajectory: decreasing sharply from birth to 37 weeks PMA, followed by a slower recovery from 37 weeks to one year. This pattern was seen in several memory CD4+ and CD8+ metaclusters, indicating a transiently activated T cell phenotype at birth that resolves under more homeostatic conditions. Two CD4+ ICS metaclusters (5 and 9), which were IL-8-positive, had inverted-V trajectories.

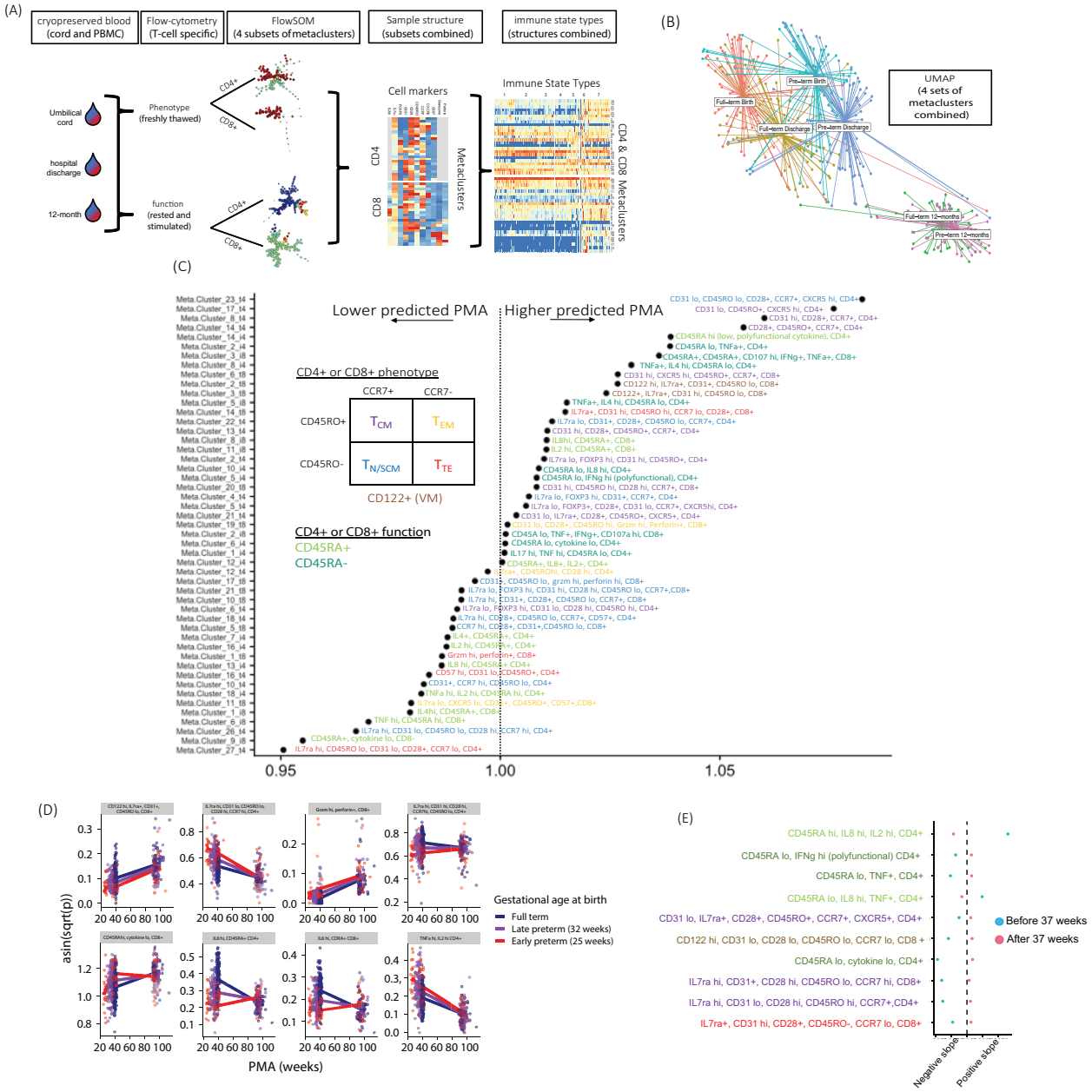

Fig. 4. Composition and patterns of prenatal and postnatal T cell phenotype and function in infants. (A) Flow cytometry was performed on blood obtained from 133 preterm and 79 full term infants at birth, at the time of hospital discharge or at 36-42 weeks postmentrual age (PMA), whichever event occurred first, and at 12 months. T cells were characterized by phenotype ("Tphe", unstimulated) and cytokine function ("ICS", stimulated *in vitro*). Cell metaclusters were identified using the Flowsom clustering algorithm. (B) Uniform manifold approximation and projection (UMAP) was used for dimensional reduction (each dot on the UMAP display represents a sample). Color overlays in UMAP show age cohort and timepoint. (C) Individual T cell metaclusters found to have a linear correlation with PMA are displayed left to right in chronologic order of PMA association. T cell phenotype subpopulations are grouped and colored based on CCR7 and CD45RO expression (TCM=central memory, TEM=effector memory, TN/SCM=naive, stem cell memory, TTE= terminal effector) and CD122 (IL-2rβ, VM=virtual memory). T cell functional phenotypes (cytokine profile) are colored based on positive CD45RA expression (naïve, light green) or low CD45RA expression (activated/memory, dark green). (D) Line graphs are shown for select populations enriched in either preterm (red, purple) or full term subjects (blue). (E) Longitudinal pattern of metacluster expression was tested for significant nonlinear trajectory across three timepoints (v-shaped or inverted v). Blue dots represent birth to discharge, pink dots show discharge to one year. Positioning of subpopulations to the left of dotted line indicates a negative slope (decreased expression) and to the right indicates a positive slope (increased).

Defining immune state types

To characterize T cell trajectory during infancy, we partitioned samples into immune state types (ISTs) based on the abundances of all metaclusters, using the same DMM modeling technique that was applied to the microbiota samples. We defined 7 T cell phenotype immune state types (Tphe ISTs) and 8 ICS immune state types (ICS ISTs), which were numbered according to their order of occurrence and exhibited strong associations with PMA (ANOVA, r^2= 0.86 and 0.69, respectively) (Fig. 5A-5D). Tphe1-Tphe4 and ICS1-ICS4 were only seen in samples drawn at birth and discharge. The phenotypic and functional trajectory revealed by ISTs is consistent with that found using individual metaclusters (Fig 5E-F).

Two Tphe ISTs (Tphe5 and Tphe6) were present at all three timepoints and in both GA groups, suggesting that clinical exposures, as opposed to development, drive the phenotypes. Tphe5 was most notably marked by the abundance of atypical early activated (CD31+, CD45RO-, CCR7-, CD28-) CD8+, CD4+ CM, and Treg subpopulations. Vmems were lower in Tphe5, suggesting perturbed homeostasis. This heterogeneity, reflecting activated conventional and regulatory T cells, indicates that subjects exhibiting Tphe5 at birth or discharge experienced some degree of prenatal immune priming. In fact, chorioamnionitis and/or exposure to antenatal antibiotics raised the odds of a subject ever entering Tphe5 by 7-fold (95% CI 1.0-54, $p<.05$) and 4-fold (95% CI 1.1-13, $p<.03$), respectively, in a joint logistic regression model that adjusted for GA, sex, race, mode of delivery, and premature rupture of membranes (Supplementary Fig. 4). Tphe6, which was more common at 12 months, was marked by high abundance of CD57+ and cytotoxic CD8+ metaclusters. CD57+ CD8+ T cells have been associated with T cell exhaustion due to chronic viral infection (23, 24). In our cohort 60% of subjects ever entering Tphe6 tested positive for CMV at 6 or 12 months, while CMV occurred in less than 7% of Tphe6 negative

subjects (odds ratio 10.2, p<.0001). These results demonstrate the utility of T cell clustering to distinguish atypical from normal T cell developmental trajectory, and in identifying clinical factors that perturb normal immune development in infants.

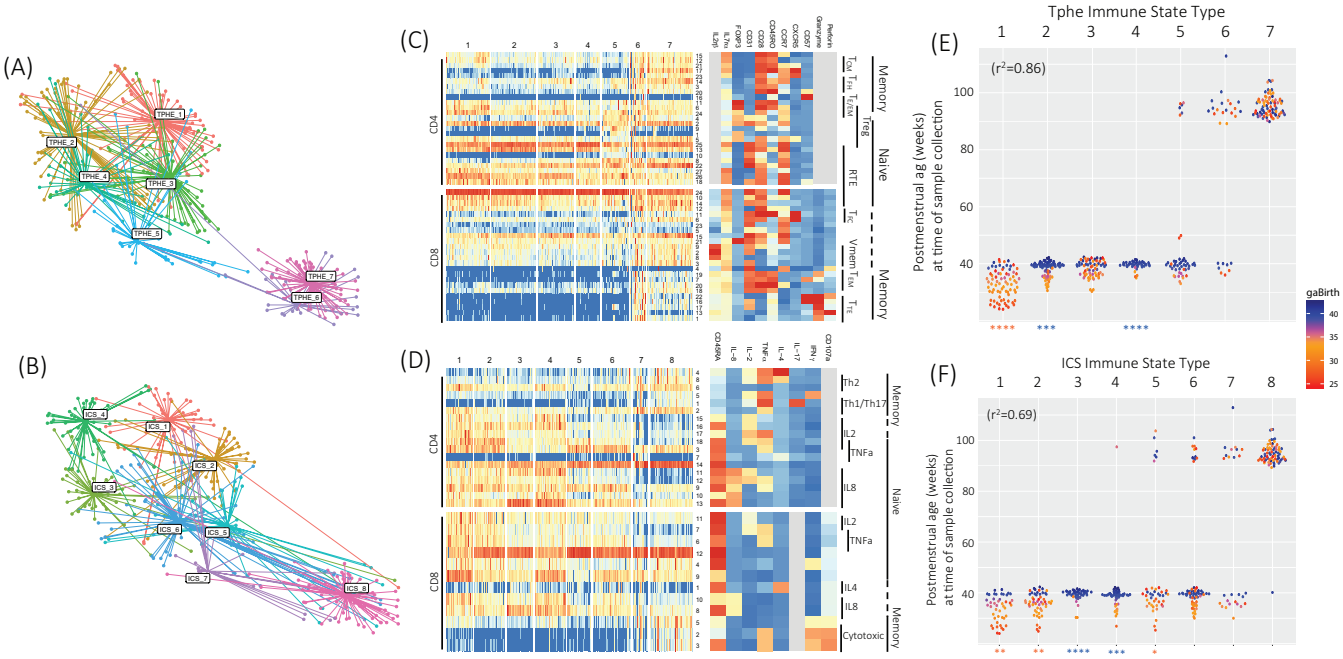

Fig. 5. Construction of immune state types. Separate T cell phenotype (A, top row) and T cell function (B, bottom row) immune state types (ISTs) were defined based on metacluster abundances and used to color UMAP projections of all samples. (C) Tphe and (D) ICS IST composition and metacluster feature abundance. (E) Tphe and (F) ICS ISTs were sequentially numbered according to the average postmenstrual age at which they occurred. PMA at sampling along y-axis, colored by gestational age at birth. Asterisks at base of dot plots indicate significant enrichment for either preterm (orange) or full term (blue) samples (*p<0.05, **p<0.01, ***p<0.001, ****p<0.0001).

Early-life immunity and subsequent microbiome state type

We next hypothesized that some immune and microbial features would exhibit correlations beyond what their mutual dependence on host age could explain. In order to test this, we modeled the number of days a subject spent in a given CST and the odds the CST occurring in a subject at all each as a function of one of their immunological parameters (IST or

metacluster abundance at a particular time point), adjusting for gestational age at birth and mode of delivery. We fit models on all pairwise combinations of CSTs and immunological parameters. The significant results of these tests were visualized as networks (Fig. 6A, Supplementary Fig. 5A). Among the models of CST duration, of the potential 6318 possible associations between the 26 CSTs and 243 immunological parameters, only 10 Tphe and no ICS metaclusters achieved statistical significance after multiple test correction. CST-associated CD4+ metaclusters preceded, but CD8+ metaclusters followed, the average onset of their associated CST, suggesting the directionality of these relationships. Among the models of whether or not a CST would occur at all, of the 15 total ISTs, only 3 (Tphe1, Tphe3 and Tphe5) were significantly correlated with a single CST (nCST 8). The most striking finding in the network was that early entry into Tphe5 (n=25 subject-samples) precluded a subject ever entering into nCST 8 (Fig. 6B). The nCST 8 dominant taxa *Allociococcus* was virtually absent in preterm samples collected prior to 40 weeks PMA, but appeared soon after, with stationary mean abundance post-discharge (Fig. 6C).

We then performed a similar analysis fitting survival models using the same covariates and time to first reach a given CST as the outcome. Interestingly, gCSTs, CD8+ T cell populations and ICS metaclusters appeared significant more often in these models than in the duration and occurrence models (Supplementary Fig. 5B). Infants with higher TNFα or IFNγ+ naïve CD8+ T cell metacluster frequencies at discharge and one year showed delayed entry into the *Streptotoccus*-dominant nCST 4. The gCST 9 (*Bifidobacterium* and *Bacterioides* low), in which there were a higher number of PT samples, was delayed in subjects discharged with higher frequencies of effector CD8+ populations. Similarly, the occurrence of gCST 3, the most diverse and mature gCST common prior to discharge and the earliest gCST in which *Clostridia* are

prevalent, was accelerated in subjects exhibiting Tphe2 at discharge (Supplementary Fig. 6). These results indicate that precocious T cell function may impact developmental timing and rate of progression of the gut microbiota, rather than promoting persistent differential abundance of specific taxa as is observed in the airway.

Illness, Microbiome and Nascent T Cell Immunity

Previous reports indicate that *Alloiococcus* in the respiratory tract is positively associated with antibiotic-resistant otitis media, but also with less severe respiratory illness in children (25, 26). Because the predominance of *Alloiococcus* is the distinguishing feature of nCST 8, and the occurrence of nCST 8 was precluded by the occurrence of Tphe5 in early life, we sought to assess the relationship between *Alloiococcus* abundance in the nose, acute respiratory illness, and early immunopheotype, controlling for multiple confounders. To identify episodes of respiratory illness post-NICU discharge, infants were scored by parents using a self-reported modified COAST score when respiratory symptoms arose (27). If the threshold of 3 was met, an in-person study visit was initiated, during which symptom scores were reviewed, nasal and rectal swabs were obtained, and a physical exam was performed.

As expected, the Tphe5 immunophenotype at birth or discharge was associated with diminished *Alloiococcus* abundance in the nose across all post-discharge timepoints, yielding a 7-fold reduction (3-14 fold, 95% CI, p-value < 0.001; Fig. 6C), while controlling for day of life, gestational age at birth, mode of delivery, and repeated sampling of subjects. Additionally, we found a 40% reduction in the odds of a sample being taken during acute illness for every 10% increase in *Alloiococcus* relative abundance (log odds = -3.52 ± 2.19, 95% CI, p-value = 0.002), controlling for confounders as above. Considering the joint effects of acute illness and Tphe5

occurrence at birth or discharge as predictors in the same model, we found that both were associated with reduced *Alloiococcus* abundance, (log ratios -0.91 ± 0.42 and -1.90 ± 0.80, respectively, 95% CI; p-values < 0.001; Fig. 6D). However, despite negative associations between Tphe5 and *Alloiococcus* abundance, and *Alloiococcus* abundance with illness, Tphe5 was not significant as a predictor of illness, either by itself (log odds = 0.54 ± 0.70, 95% CI, p-value = 0.131) or in conjunction with *Alloiococcus* relative abundance (log odds = -0.35 ± 0.71, 95% CI, p-value = 0.328), controlling for confounders in both cases. Together, these results show that early immune priming, as seen by early entry into Tphe5, may shape respiratory microbiota development, which is subsequently strongly linked with acute respiratory illnesses.

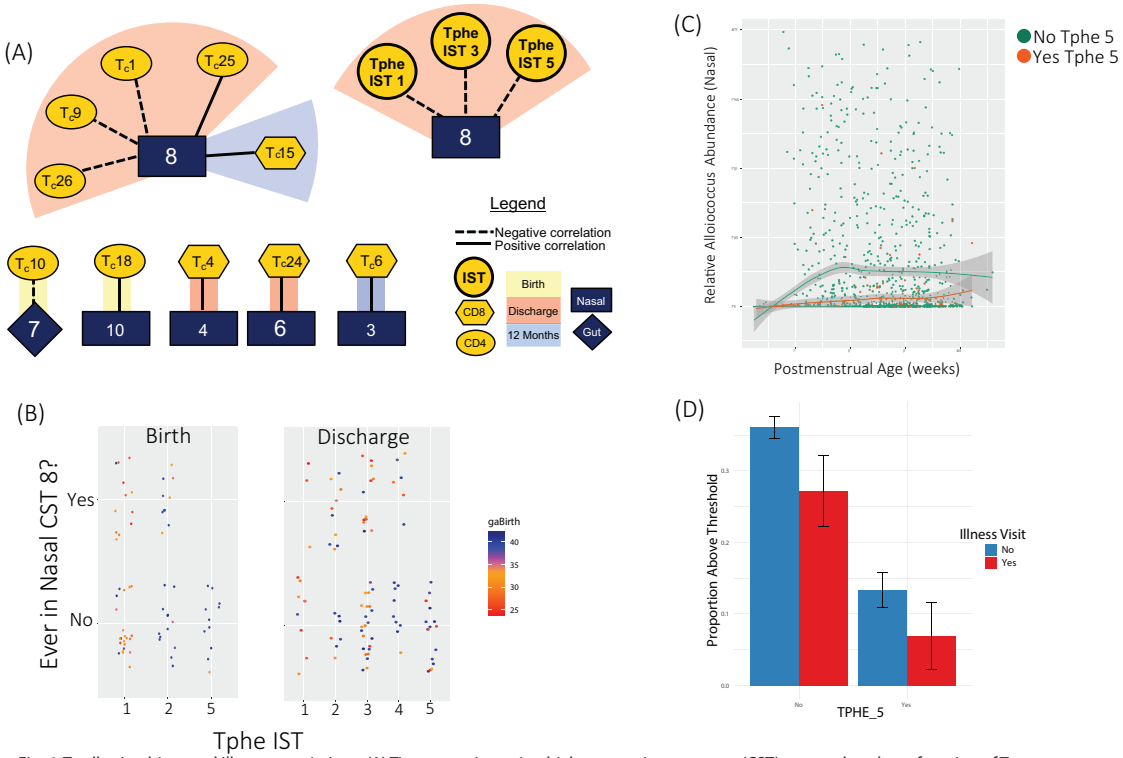

Fig. 6. T cell-microbiota and illness associations. (A) Time spent in a microbial community state type (CST) was analyzed as a function of T cell features (using both metaclusters and ISTs), controlling for gestational age at birth and more of delivery (significant associations shown using 10% FDR). (B) Birth and discharge samples were plotted based on their T cell IST, and grouped based on whether or not the subjects ever subsequently entered nCST 8. Sample color indicates gestational age at birth. Subjects in Tphe5 at these early time points never subsequently entered into nCST 8. (C) Relative abundance of nCST 8 dominant genus, *Alloiococcus* (y-axis) is shown for subjects with (orange) or without (green) Tphe5 immunophenotyped at birth or discharge. Points are positioned along x-axis based on the PMA at which sample was obtained. (D) Nasal samples were grouped along the x-axis based on whether or not a subject exhibited Tphe5 at birth or discharge, and further segregated based on whether they were taken during illness (red) or surveillance (blue). Bar height indicates the proportion of samples (+/- 95% C.I.) within each group with *Alloiococcus* relative abundance above 5%.

Immune/Microbial Developmental Index and Respiratory Outcome

Observing that rare T cell-microbiota interactions occurring independently of PMA impacted respiratory morbidity led us to hypothesize that mistimings in development of T cells or microbiota increased the risk of PRD. To test this hypothesis, we developed a quantitative model of "normal" PMA, as a function of T cell and microbiota composition. We trained two sparse regression models that used the metacluster and OTU abundance vectors to predict log2-transformed PMA at sample collection. Holding out a subject's longitudinal record, the cross-validated models strongly predicted PMA using either T cell metaclusters (r^2=0.77) or bacterial taxa (r^2=0.65) (Fig. 7A). For each subject, the fitted intercepts of these models – predicted PMA at 37 weeks actual PMA – indicate the subject's microbiota and T cell maturity relative to normal at term equivalent. The fitted slopes of the models indicate a subject's *rate* of microbiota and T cell maturation over the first year, again relative to normal. These four fitted parameters define a *developmental index* (DI) for each subject, which was used to assess mistiming and asynchrony in T cell and microbiota development.

We used random forest classification models to compare the predictive power of DI alone to that of a set of known clinical risk factors for PRD. The clinical features were race, maternal education, sex, GA at birth, birthweight, season at birth and oxygen supplementation integrated over the first 14 days of life. The four developmental index features were the z-scores of the microbiota and T-immune slopes and intercepts. In cross-validation, the clinical features predicted PRD with area under the curve (AUC) of 0.69 (0.59-0.79 95% CI). Not surprisingly, the features that contributed most to the outcome were increased oxygen exposure, lower birthweight and younger gestational age at birth (Supplemental Fig. 7). When compared to clinical predictors, the developmental index had statistically equivalent skill in predicting PRD

(Fig 7B, AUC 0.64, 0.54-0.74 95% CI). Combining the clinical features and the developmental variables did not improve the predictive model, further evidence of early life exposures causing

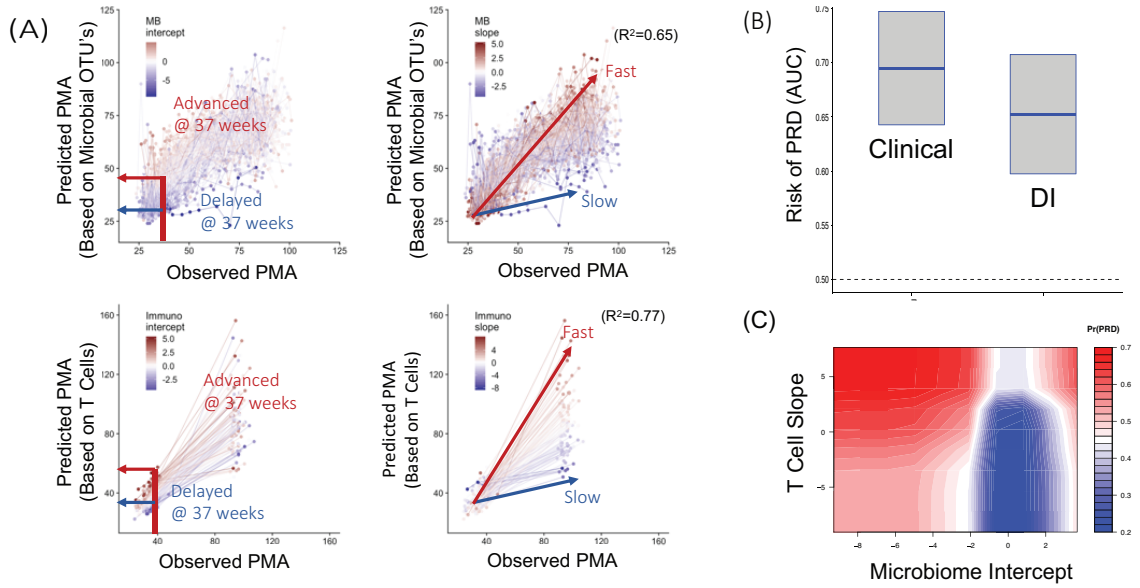

Fig. 7. Microbiota and Immunologic Developmental Index and Respiratory Outcome. Elastic net regression was used to predict postmenstrual age (PMA) based on T cell populations and microbial operational taxonomic units (OTUs). (A) Dots connected by lines represent an individual subject's samples. The predicted age of a subject is plotted against the observed age at the time of sampling. The "Developmental Index" was constructed using both the intercept at 37 weeks (left) and slope of T cell and OTU maturation (right). Z-scores for each subject are displayed as color overlays (red indicating relatively advanced PMA and faster development, and blue indicating relatively delayed PMA and slower development). (B) A random forest machine learning algorithm was used to predict PRD from clinical variables ("Clinical"), Developmental Index of T cells and microbiota ("DI"). Box plots show mean and confidence interval of the area under the curve calculated for each set of variables. (C) Of the four components of DI (T cell slope and intercept, microbiota slope and intercept) the contour graph shows the combination with the best PRD predictive strength, controlling for clinical factors: microbiota intercept and T cell slope. Blue indicates lower PRD risk, red indicates higher risk.

durable effects on T cell and microbial development. Of the four components generating the DI, the microbiome intercept and immune slope had largest variable importance scores. In exploring the functional relationship between PRD and these factors, we observed that immature microbiota at term equivalent PMA increased the risk of PRD by over 2-fold, and this effect was magnified in subjects with accelerated T cell maturation (Fig. 7C). Together with the Tphe5-*Alloiococcus* findings, these results support the notion that timing of T cell and microbiome maturation relative to an infant's age play an integral role in promoting or interfering with respiratory health.

Discussion

Birth marks the commencement of a dynamic interplay between innate developmental programming, colonization and assembly of the microbiome, and differentiation and maturation of the adaptive immune system which influences health from infancy through adulthood. In healthy infants, this process balances the accommodation of commensal microbiota, appropriate immune response to pathogens, and functional maturation of the organs at the interface between human host and environment. By developing longitudinal models of microbiota composition and T cell populations, we were able to establish conceptually and analytically tractable representations of these systems, and to interrogate their maturation and development, revealing several key findings. First, T cells and microbiota exhibit structured patterns of progression synchronized by postmenstrual age, with pronounced differences between pre- and full-term infants in very early life and a tendency towards convergence by the end of one year. Furthermore, within the framework of development driven by PMA, interactions occur between T cell population profiles and microbiota community structure. Finally, atypical or asynchronous immune and microbiota development are markers of respiratory disease and health outcomes. To our knowledge, this is the first study to successfully model the influence of this triad of T cell, microbiota, and host development on clinical outcomes in a cohort of both preterm and full-term human infants.

The ability to predict a subject's PMA based on their T cell phenotype is strong evidence that developmental state is a key driving factor in immune maturation, which is further reinforced by convergence of PT and FT phenotypes over time. Characterizing the immune trajectory during infancy revealed greater heterogeneity than previously appreciated, especially between PT and FT subjects and even within their predominantly naïve T cell pool. As an

example, early PT and FT ISTs were both enriched for naïve T cell subpopulations with high CCR7 and CD28 and low CD45RO expression. Yet, CD31, IL-7rα and CXCR5 naive metaclusters were differentially abundant between PT and FT, implicating differences in cell survival and provision of B-cell help. Our results are aligned with previous studies demonstrating that PT infants have higher proportions of CD45RO+ T cells in their cord blood (28, 29). Many of the PT-enriched CD4+ CD45RO+ subpopulations, however, were of a Treg phenotype, confirming prior studies showing that activated fetal naive T cells have a propensity towards Treg differentiation (30) (31). The low abundance of virtual memory cells in PT subjects at birth is contrary to earlier speculation that in utero T cell activation in PT is caused by homeostatic expansion alone (32-34). The direct correlation between gestational age and IL-8+ T cells is notable in that the Olin study shows enhanced plasma IL-8 in PT when compared to FT (14). Our focus on T cells specifically, rather than secreted mediators in plasma, sheds light on a T cell-specific trajectory during infancy that may be distinct from the innate compartment and is largely, but not entirely, dependent on postmenstrual age.

Our results also reinforce the central role of host development in driving microbiota progression over time, with premature infants exhibiting distinct patterns of microbiota composition in very early life and a convergence between pre- and full-term infants over the first year. Despite this general tendency towards convergence in T cells and microbiota, the occurrence of certain state types reflect an enduring influence of GA (e.g. gCST 4, 6, and 8, nCST 8 and 12, and early ISTs) and clinical exposures (Tphe5 and Tphe6), indicating that pre- or perinatal events can have persistent effects which disrupt the maturation process and alter developmental trajectories.

Together, the microbiota of the airway and gastrointestinal tract, and their interaction with one another and with host immune function, constitute the gut-lung axis, a system increasingly implicated in respiratory morbidity (35, 36). Notably, while the relationship between immune development and the gut microbiome has featured prominently in literature, we identified more, stronger associations between T cell populations and nasal microbiota. Of particular interest is the association observed between the occurrence of Tphe5 early in life (at birth or discharge), and the subsequent abundance of *Alloiococcus* in the nose. *Alloiococcus* is a common post-discharge colonizer, but its abundance is dramatically reduced in infants who pass through Tphe5 early in life, with nCST 8 – the *Alloiococcus* dominated nCST – being entirely absent from these subjects. The additional observation that *Alloiococcus* is substantially diminished during acute respiratory illness reveals a previously undescribed connection between T cell development at birth, post-discharge airway colonization, and susceptibility to respiratory infection throughout the first year of life.

By defining developmental indices based on microbiota and T cell populations, we establish that maturity at term and rate of maturation over the first year are indicators of disease outcome at one year (PRD). Specifically, precocious immune development in conjunction with an immature microbiome at term corresponds to substantially elevated risk of PRD, while either one of these factors by themselves has an attenuated effect. This indicates that mistimed or discordant maturation between the microbiome and immune system is a correlate of respiratory morbidity. Previous reports have used age, microbiota, or immune variables as independent factors in predicting respiratory outcome (2, 5, 25, 37). These studies do not address the possibility that a newborn's immune system is not simply deficient, but rather under normal developmental conditions, is uniquely balanced to provide protection against novel pathogens

while minimizing immunopathology. Exposures that accelerate or delay the normal maturation of T cells and microbiota during infancy, such as in utero infection promoting the early occurrence of Tphe5, may disrupt this age-specific balance that has served human evolution so well.

The PRISM study results demonstrate the strength of large, prospective observational studies in discovering early risk factors for disease. There are also limitations to our study design that should be acknowledged. The greatest challenge in conducting immune surveillance studies in newborns is obtaining sufficient blood volumes to perform comprehensive assays and adequate sampling frequencies to inform robust longitudinal models. Our results show that substantial changes in the immune system occur between NICU discharge and 12 months, and without the benefit of intensive interim sampling, it is difficult to comprehensively account for all clinical factors that may shape an individual's immune trajectory. However, our discoveries can be used inform future studies focusing on the timing and specific shifts in immune populations and microbiota that impact respiratory outcomes, such as Tphe5 and *Alloiococcus*. It will also be important for future models to address other events, including distinguishing respiratory viral infections and changes in nutrition, and how these exposures either coordinate or interfere with normal developmental trajectories. Despite the inherent challenges, using human observational studies is a powerful approach to scientific discovery which can reveal practical insights into the systems influencing health and disease that are not readily accessible in controlled experimental settings or animal models. However, translation of these discoveries into medical management will benefit from carefully controlled interventional studies. Specifically, our results suggest markers of immune and microbiota development which may indicate susceptibility to respiratory infection and risk of chronic respiratory morbidity. Additionally, the

interaction between these two systems invites the possibility of intervention, whereby biotic therapy or immunotherapy applied to one system could potentially be used to modulate the other. Finally, the evidence that an infant's health is influenced by the these two systems remaining synchronous with postnatal development underscores the need to tread cautiously when considering interventions that may disrupt this normal balance.

Materials and Methods

Study Design

All study procedures were approved by the University of Rochester Medical Center (URMC) Internal Review Board (IRB) (Protocol # RPRC00045470 & 37933) and all subject's caregivers provided informed consent. The infants included in the study were enrolled within 7 days of life for the University of Rochester Respiratory Pathogens Research Center PRISM and cared were for in the URMC Golisano Children's Hospital. Clinical data including nutrition, respiratory support, respiratory symptoms, medications, comorbidities, were entered into REDCap (37, 38), then integrated with laboratory results using the URMC Bio Lab Informatics Server, a web-based data management system using the open source LabKey Server (39). Blood was collected at birth, time of NICU discharge or 36-42 weeks PMA (whichever occurred first), and at 12 months of life. We collected 2729 gut (842 from NICU and 1887 post-discharge), and 2210 nasal (619 from NICU and 1591 post-discharge) usable microbiota samples longitudinally from 139 pre-term and 98 full-term infants. From the PRISM study cohort, fecal (rectal) and nasal material was collected from pre-term infants (23 to 37 weeks gestational age at birth

(GAB)) weekly from the first week of life until hospital discharge, and then monthly through one year of gestationally corrected age. Rectal and nasal samples were collected from full-term infants at enrollment and monthly through one year. Additionally, rectal and nasal samples were collected from all infants whenever they exhibited symptoms of acute respiratory illness after discharge from the hospital. Symptoms of acute respiratory illness prompting sample collection were summarized by the primary caregiver using a symptom COAST (Childhood Origins of Asthma) score sheet (1). Parents were instructed to notify the study team if the infant had symptom score of three or greater. All blood samples generating usable data were included in all analyses. For training the PMA predictions models (described below), all microbiota samples were used. For all other analyses, microbiota samples from subjects that did not have any usable data from blood were excluded.

Flow Cytometry Methods

Sample collection, isolation, storage, thawing, stimulation and staining for flow cytometry was performed as detailed in a previously published method (40). In short, cord blood and peripheral blood mononuclear cells were isolated via Ficoll centrifugation, cryopreserved and stored in liquid nitrogen, and rapidly thawed and washed with pre-warmed RPMI-1640 (10% FBS and 1x L-glutamine); thawing was done in 'subject-balanced' batches (equal mix of pre and full-term subjects, each with three time points) and an aliquot of each freshly thawed sample was plated and stained with a T-cell phenotyping ('Tphe') panel with the remainder of the sample rested overnight in an incubator, plated and stimulated with *Staphylococcus aureus*, Enterotoxin Type B (SEB), and stained with a T-cell functional panel ('ICS'). Panel compositions are as shown in (Supplementary Fig. 1).

Samples were acquired on a BD LSRII (core facility instrument QC-ed daily with BD CS&T beads); PMT voltages normalized per run to pre-determined/optimized 'Peak-6' (Spherotech) median fluorescence values. R-based packages and scripts were used for all post-acquisition processing and analysis. Reading of raw .fcs files, compensation, transformation, and subsetting/writing of .fcs files was performed using flowCore (41). To minimize inter-run variation associated with the Tphe panel, the flowStats (42) warpSet function was used to normalize arcsinh transformed channel data using a healthy donor adult PBMC control as reference. For analysis with the clustering algorithm FlowSOM, an iterative approach was used for both panels to first cluster on live, intact, lymphoid-sized CD4+ and CD8+ T-cell subsets (in the case of the ICS panel, including activated (CD69+) subsets); those subsets were then re-clustered to capture rare populations and optimally resolve phenotypic heterogeneity and associated function. Over-clustering followed by expert-guided merging was favored when defining the number of final metaclusters. Metaclustering results used in downstream analysis were represented as proportion of the respective T-cell subset, per sample. All scripts, including Tphe arcsinh cofactors, warpSet and FlowSOM parameters, and final clustering counts are available in (Supplementary R-Code and Supp. Fig. 2).

Microbiota Identification

Microbiota sample collection and storage techniques, genomic DNA extraction and background control methods were as previously published (7). Raw data from the Illumina MiSeq was first converted into FASTQ format 2 × 312 paired-end sequence files using the bcl2fastq program (v1.8.4) provided by Illumina. Format conversion was performed without de-multiplexing, and the EAMMS algorithm was disabled. All other settings were default. Samples

were multiplexed using a configuration described previously (43). The *extract_barcodes*.py script from QIIME (v1.9.1) (44) was used to split read and barcode sequences into separate files suitable for import into QIIME 2 (v2018.11) (45) which was used to perform all subsequent read processing and characterization of sample composition. Reads were demultiplexed requiring exact barcode matches, and 16S primers were removed allowing 20% mismatches and requiring a matching window of at least 18 bases. Cleaning, joining, and denoising were performed using DADA2 (46): reads were truncated (forward reads to 260 bps and reverse reads to 240 bps for rectal V3-V4 samples and forward reads to 275 bps and reverse reads to 260 bps for nasal V1-V3 samples), error profiles were learned with a sample of one million reads per sequencing run, and a maximum expected error of two was allowed. Taxonomic classification was performed with custom naïve Bayesian classifiers trained on target-region specific subsets of the August, 2013 release of GreenGenes (47). Sequence variants that could not be classified to at least the phylum level were discarded. Sequencing variants observed fewer than ten times total, or in only one sample, were discarded. Rectal samples with fewer than 2250 reads and nasal samples with fewer than 1200 reads were discarded. Phylogenetic trees were constructed for each body site using MAFFT (48) for sequence alignment and FastTree (49) for tree construction. For the purposes of β-diversity analysis, rectal and nasal samples were rarefied to depths of 2250 and 1200 reads, respectively, and the Unweighted Unifrac (50) metric was applied.

Statistical analyses

CST and IST Assembly. Microbial community state types (CSTs) were defined for each body site by fitting Dirichlet multinomial mixture (DMM) models (51) using the R package DirichletMultinomial (v1.22.0) (52, 53), R version 3.5.0. Sample composition was represented

using normalized counts of the most specific operational taxonomic units (OTUs) present in at least 5% of the samples from a given body site. Normalization was performed on a per sample basis by taking the relative abundance of each OTU and multiplying by 2250 for rectal samples and 1200 for nasal samples. Resulting non-integer counts were rounded down. For each body site, the DMM model was fit with one through twenty Dirichlet components and the optimal number of components was selected by minimizing the Laplace approximation of the negative-log model evidence. In this model, CSTs are synonymous with Dirichlet components, and each sample was assigned to the CST from which it had the highest posterior probability of be derived. This procedure was repeated with the immunological data in order to define immune state types (ISTs), using relative abundances of FlowSOM defined Metaclusters in the place of OTUs. Relative abundances were computed within assays (TPHE and ICS) and major populations (CD4 and CD8) separately, and converted to counts by multiplying by 50,000 and rounding down. CD4 and CD8 counts were combined to fit the DMM for each assay.

Microbiota-T cell Associations. Associations between microbiome development and the immune system were modeled using microbiome CST occurrence patterns as outcome variables and iterating through the relative abundances of each FlowSOM metacluster or observed IST at each time point as predictors. In symbols, we used the model

CST ~ immune_parameter + MOD + GA + (sampling_intensity).

For each CST, each of these immunological parameters (metacluster relative abundances and IST) at each of the three time points when the immune system was sampled (birth, discharge, and one year) was assessed independently, and are hereafter referred to as the immunological variables of interest (VOIs).

CST occurrence patterns were related to immunological VOIs by testing three types of associations between every CST-VOI combination at the level of individual subjects, while controlling for mode of delivery (MOD), gestational age at birth (GAB) and, in model (i) only (see below), the number of microbiome samples (sampling_intensity) that were collected from an individual. These models differed in the aspect of CST occurrence that was modeled as the outcome. Model (i) tests associations between the VOI and whether or not a CST occurs at all in an individual; (ii) tests associations between the VOI and how persistent a CST is in an individual; and (iii) tests associations between the VOI and the days to first occurrence of a CST in an individual. Model (i) was tested using logistic regression with VOI, MOD, GA and the number of microbiome observations from a given individual as the sampling intensity. The outcome indicated whether or not a given CST was ever observed in the individual. We tested the VOI association by dropping that term and calculating a likelihood ratio test. Model (ii) was tested using a quasi-Poisson regression model with MOD, GA, and the VOI as covariates, and total number of days the subject was assigned to *any* CST as an offset. The number of days a subject was assigned to a given CST was the outcome and was calculated by summing the interval lengths between CST change points. Intervals were calculated from midpoint to midpoint on the sampled days of life. At birth, subjects were placed in the first observed CST if the first sample occurred within 14 days of life, otherwise the first interval was excluded. Subjects were assumed to remain in their final observed CST for an interval equal to half the interval length between the penultimate and ultimate sample. Significance of the VOI was assessed as in model (i). Model (iii) was tested using interval censored, accelerated log logistic failure time models (R package icenReg v2.0.9) (54) with MOD, GA, and the VOI as covariates and the interval preceding the first observation of a given CST as the outcome. For gCST 1 and

nCST 1, which on average were the earliest CSTs, we modeled the interval preceding the first observation of a CST other than NAS 1 or REC 1. For each CST, only subjects that were ever observed in that CST at some point were included. Significance was assessed based on Wald test p-values of the terms in the fitted full models.

For models (i)-(iii), subjects with fewer than one sample taken per 30 NICU-days or fewer than six samples post discharge were excluded. We filtered immune VOI with fewer than ten observations, and CSTs present in fewer than 10% of the remaining observations. Numerical covariates were converted into z-scores, except GA which we modeled as $(\mathrm{GA} - 37)/37$. Within each model (i)-(iii), multiple testing across all CSTs and VOIs was corrected for using the Benjamini-Hochberg method at 10% FDR.

Tphe5, Alloiococcus abundance, and acute illness associations. Using only post-discharge nasal samples, the abundance of *Alloiococcus* represented as read counts was modeled as a function of day of life, GA, MOD, and the occurrence of Tphe5 at birth or discharge using a generalized estimating equation fit with the geeglm function in R (55). Subject was used as the clustering variable, an exchangeable working correlation structure was specified, total reads per sample was used as an offset, and the family was Poisson with a log link function. This model was repeated with the addition of acute illness as a covariate. The probability of a sample coming from an illness or healthy surveillance visit was modeled using mixed effects logistic regression fit with the glmer function (56), using *Alloiococcus* relative abundance, DOL, GA, and MOD as covariates, with Subject as a random effect. This model was repeated with the addition of Tphe5 at birth or discharge as a covariate.

Prediction of PMA. Two separate elastic net regression models (57) were trained to predict (58) the log2-transformed PMA with a) T cell immunological features and b) microbial

abundance. In (a) the four feature sets were CD4 ICS, CD8 ICS, CD4 Tphe and CD8 Tphe meta clusters, while in (b) the two feature sets consisted of nasal and rectal species-level relative abundances from samples collected prior to DOL 450, filtered to remove taxa present in fewer than 3% of samples. A total of 433 samples from 185 subjects and 80 features were included in (a). Model (b) was trained on 3032 samples from 237 subjects and 218 features. Some samples had incomplete feature sets, e.g., if only the ICS panel was run then both the CD4 and CD8 Tphe sets were missing, or if only the nasal microbiome was sampled and the rectal abundances were missing. We treated this as a missing data problem, and imputed the values with their mean values among non-missing cases. Imputation was chained onto the elasticnet model (occurred only using the training data, in each fold) for the purposes of tuning and validation. Within each feature set, we used the relative proportions, transformed into z-scores.

Cross validation for tuning and prediction. We tuned the model and estimated its performance using cross-validation by holding out a subject's entire longitudinal record. We tuned the elastic net alpha in [0, 1] and lambda in [.001, .5] parameters by randomly selecting 50 combinations of (alpha, lambda) and evaluating the test mean-square error (MSE) via 5-fold cross-validation. After finding a minimizing pair of (alpha, lambda), the model was refit with 10-fold cross-validation. For each subject i, this provides two sequences of fitted values, representing the log2-transformed PMA prediction. For instance, for the microbiome, we have

$$\widehat{Y_{ij}} = f^{-i}(x_{ij}), j = 1, \dots, n_i,$$

where x_{ij} represent microbial feature vectors, n_i indexes the number of longitudinal samples for subject i, and f^{-i} represent the elastic net model trained excluding subject i. For the

T cell immunome, the analogous model is fit. The back-transformed values $2^{\widehat{Y_{ij}}}$ were used to calculate each model's R^2.

Immunological and microbial developmental indices. The longitudinal sequence of cross-validated fitted values $\widehat{Y_{ij}}$ were compared to the true PMA for each subject using a linear mixed model. We fit the model

$$\hat{Y} - \log_2(37) \sim \log_2(\text{PMA}/37) + (1 + \log_2(\text{PMA}/37)|\text{Subject})$$

thus $\widehat{Y_{ij}} = \alpha_i + \beta_i \times \text{PMA}_{ij} + \epsilon_{ij}$ and calculated the best linear unbiased predictor of each subject's 37-week intercept α_i, slope β_i and their conditional standard errors se(α_i), se(β_i). These are transformed into a quantity similar to a z-score by subtracting the median of α_i, β_i over subjects i, and dividing by its conditional standard error se(α_i) or se(β_i).

Prediction of PRD. We used random forest classification models to predict PRD using two feature sets: clinical and developmental index. The clinical features were race, maternal education, the baby's sex, gestational age, weight and season at birth, and oxygen supplementation integrated over the first 14 days of life. The developmental index features were the z-scores of the microbiome and T-immune slopes and intercepts. The random forest hyperparameters mtry, ntree and nodesize were tuned separately for each feature set with random search using 5-fold cross-validation. After the optimal parameters were found for each feature set, a second round of 20-fold cross validation was used to evaluate the area under the ROC curve (AUC). The fitted values from the random forest regression were calculated using the function generatePartialDependenceData.

Acknowledgments:

Authors would like to acknowledge the University of Rochester Pediatrics Translational Biospecimen Laboratory, the University of Rochester Genomics Research Core, the Flow Cytometry Core, and the Human Immunology Center. We also thank Richard Simon (The Harley School), for his assistance with figure preparation and graphic design. This study was dependent on the nurses and staff at the Golisano Children's Hospital NICU and URMC Strong Beginnings Maternity Services, and most of all to our families who generously consent to research studies.

Funding:

NIH NIAID HHSN272201200005C (Respiratory Pathogens Research Center)

NIH NIAID 1K08AI108870-01A1 (CD8 T Cell Dysregulation in Premature Infants)

NIH NHLBI U01 HL101813-01 (Prematurity and Respiratory Outcomes Program)

NIH NCATS UL1 TR000042 (Clinical and Translational Science Institute)

Author Contributions:

Conception, execution, interpretation and manuscript preparation: KMS, AM, AG, NL, GSP, MC, AD

Project PI's, University of Rochester: GSP, MC, SG, AF, DJT

Acquisition and analysis of experimental data: NL, AG, AG, HK, JC, AG, KMS

Clinical and sample data collection, study coordination and recruitment: HH, GSP, MC, KMS

Biostatistical analysis: AM, AG

Clinical and laboratory data integration and management: JHW, SB

Data and Materials Availability:

Annotated datasets for 16S sequencing and flow cytometry results can be found in dbGaP, SRA and Immport, accession number phs001347. Code is available at https://github.com/amcdavid/CoordinatedTCellsMicrobiota.

References:

1. Busse WW, Lemanske RF, Jr., Gern JE. Role of viral respiratory infections in asthma and asthma exacerbations. Lancet. 2010;376(9743):826-34. Epub 2010/09/08. doi: 10.1016/S0140-6736(10)61380-3. PubMed PMID: 20816549; PMCID: PMC2972660.

2. Tregoning JS, Schwarze J. Respiratory viral infections in infants: causes, clinical symptoms, virology, and immunology. Clin Microbiol Rev. 2010;23(1):74-98. Epub 2010/01/13. doi: 10.1128/CMR.00032-09. PubMed PMID: 20065326; PMCID: PMC2806659.

3. Inoue Y, Shimojo N. Epidemiology of virus-induced wheezing/asthma in children. Front Microbiol. 2013;4:391. Epub 2014/01/01. doi: 10.3389/fmicb.2013.00391. PubMed PMID: 24379810; PMCID: PMC3863784.
4. Newton AH, Cardani A, Braciale TJ. The host immune response in respiratory virus infection: balancing virus clearance and immunopathology. Semin Immunopathol. 2016;38(4):471-82. Epub 2016/03/12. doi: 10.1007/s00281-016-0558-0. PubMed PMID: 26965109; PMCID: PMC4896975.
5. Scheible KM, Emo J, Laniewski N, Baran AM, Peterson DR, Holden-Wiltse J, Bandyopadhyay S, Straw AG, Huyck H, Ashton JM, Tripi KS, Arul K, Werner E, Scalise T, Maffett D, Caserta M, Ryan RM, Reynolds AM, Ren CL, Topham DJ, Mariani TJ, Pryhuber GS. T cell developmental arrest in former premature infants increases risk of respiratory morbidity later in infancy. JCI Insight. 2018;3(4). Epub 2018/02/23. doi: 10.1172/jci.insight.96724. PubMed PMID: 29467329; PMCID: PMC5916253.
6. Scheible KM, Emo J, Yang H, Holden-Wiltse J, Straw A, Huyck H, Misra S, Topham DJ, Ryan RM, Reynolds AM, Mariani TJ, Pryhuber GS. Developmentally determined reduction in CD31 during gestation is associated with CD8+ T cell effector differentiation in preterm infants. Clin Immunol. 2015;161(2):65-74. Epub 2015/08/02. doi: 10.1016/j.clim.2015.07.003. PubMed PMID: 26232733; PMCID: PMC4658282.
7. Grier A, McDavid A, Wang B, Qiu X, Java J, Bandyopadhyay S, Yang H, Holden-Wiltse J, Kessler HA, Gill AL, Huyck H, Falsey AR, Topham DJ, Scheible KM, Caserta MT, Pryhuber GS, Gill SR. Neonatal gut and respiratory microbiota: coordinated development through time and space. Microbiome. 2018;6(1):193. Epub 2018/10/28. doi: 10.1186/s40168-018-0566-5. PubMed PMID: 30367675; PMCID: PMC6204011.
8. Grier A, Qiu X, Bandyopadhyay S, Holden-Wiltse J, Kessler HA, Gill AL, Hamilton B, Huyck H, Misra S, Mariani TJ, Ryan RM, Scholer L, Scheible KM, Lee YH, Caserta MT, Pryhuber GS, Gill SR. Impact of prematurity and nutrition on the developing gut microbiome and preterm infant growth. Microbiome. 2017;5(1):158. Epub 2017/12/13. doi: 10.1186/s40168-017-0377-0. PubMed PMID: 29228972; PMCID: PMC5725645.
9. Korten I, Mika M, Klenja S, Kieninger E, Mack I, Barbani MT, Gorgievski M, Frey U, Hilty M, Latzin P. Interactions of Respiratory Viruses and the Nasal Microbiota during the First Year of Life in Healthy Infants. mSphere. 2016;1(6). Epub 2016/12/03. doi: 10.1128/mSphere.00312-16. PubMed PMID: 27904883; PMCID: PMC5120172.
10. Man WH, van Houten MA, Merelle ME, Vlieger AM, Chu M, Jansen NJG, Sanders EAM, Bogaert D. Bacterial and viral respiratory tract microbiota and host characteristics in children with lower respiratory tract infections: a matched case-control study. Lancet Respir Med. 2019. Epub 2019/03/20. doi: 10.1016/S2213-2600(18)30449-1. PubMed PMID: 30885620.
11. Dimmitt RA, Staley EM, Chuang G, Tanner SM, Soltau TD, Lorenz RG. Role of postnatal acquisition of the intestinal microbiome in the early development of immune function. J Pediatr Gastroenterol Nutr. 2010;51(3):262-73. Epub 2010/07/20. doi: 10.1097/MPG.0b013e3181e1a114. PubMed PMID: 20639773; PMCID: 2932839.
12. Rechavi E, Lev A, Lee YN, Simon AJ, Yinon Y, Lipitz S, Amariglio N, Weisz B, Notarangelo LD, Somech R. Timely and spatially regulated maturation of B and T cell repertoire during human fetal development. Science translational medicine. 2015;7(276):276ra25. doi: 10.1126/scitranslmed.aaa0072. PubMed PMID: 25717098.
13. Lee AH, Shannon CP, Amenyogbe N, Bennike TB, Diray-Arce J, Idoko OT, Gill EE, Ben-Othman R, Pomat WS, van Haren SD, Cao KL, Cox M, Darboe A, Falsafi R, Ferrari D, Harbeson DJ, He D, Bing C, Hinshaw SJ, Ndure J, Njie-Jobe J, Pettengill MA, Richmond PC, Ford R, Saleu G, Masiria G, Matlam JP, Kirarock W, Roberts E, Malek M, Sanchez-Schmitz G, Singh A, Angelidou A, Smolen KK, Consortium E, Brinkman RR, Ozonoff A, Hancock REW, van den Biggelaar AHJ, Steen H, Tebbutt SJ, Kampmann B, Levy O, Kollmann TR. Dynamic molecular changes during the first week of human life follow a robust developmental trajectory. Nat Commun. 2019;10(1):1092. Epub 2019/03/14. doi: 10.1038/s41467-019-08794-x. PubMed PMID: 30862783; PMCID: PMC6414553.
14. Olin A, Henckel E, Chen Y, Lakshmikanth T, Pou C, Mikes J, Gustafsson A, Bernhardsson AK, Zhang C, Bohlin K, Brodin P. Stereotypic Immune System Development in Newborn Children. Cell. 2018;174(5):1277-92 e14. Epub 2018/08/25. doi: 10.1016/j.cell.2018.06.045. PubMed PMID: 30142345; PMCID: PMC6108833.
15. Pryhuber GS, Maitre NL, Ballard RA, Cifelli D, Davis SD, Ellenberg JH, Greenberg JM, Kemp J, Mariani TJ, Panitch H, Ren C, Shaw P, Taussig LM, Hamvas A, Prematurity, Respiratory Outcomes Program I. Prematurity and respiratory outcomes program (PROP): study protocol of a prospective multicenter study of respiratory outcomes of preterm infants in the United States. BMC Pediatr. 2015;15:37. Epub 2015/04/18. doi: 10.1186/s12887-015-0346-3. PubMed PMID: 25886363; PMCID: PMC4407843.

16. Van Gassen S, Callebaut B, Van Helden MJ, Lambrecht BN, Demeester P, Dhaene T, Saeys Y. FlowSOM: Using self-organizing maps for visualization and interpretation of cytometry data. Cytometry A. 2015;87(7):636-45. Epub 2015/01/13. doi: 10.1002/cyto.a.22625. PubMed PMID: 25573116.
17. Bains I, Antia R, Callard R, Yates AJ. Quantifying the development of the peripheral naive CD4+ T-cell pool in humans. Blood. 2009;113(22):5480-7. Epub 2009/01/31. doi: 10.1182/blood-2008-10-184184. PubMed PMID: 19179300; PMCID: PMC2689049.
18. De Rosa SC, Herzenberg LA, Herzenberg LA, Roederer M. 11-color, 13-parameter flow cytometry: identification of human naive T cells by phenotype, function, and T-cell receptor diversity. Nat Med. 2001;7(2):245-8. Epub 2001/02/15. doi: 10.1038/84701. PubMed PMID: 11175858.
19. Gerlach C, Rohr JC, Perie L, van Rooij N, van Heijst JW, Velds A, Urbanus J, Naik SH, Jacobs H, Beltman JB, de Boer RJ, Schumacher TN. Heterogeneous differentiation patterns of individual CD8+ T cells. Science. 2013;340(6132):635-9. Epub 2013/03/16. doi: 10.1126/science.1235487. PubMed PMID: 23493421.
20. Buettner F, Natarajan KN, Casale FP, Proserpio V, Scialdone A, Theis FJ, Teichmann SA, Marioni JC, Stegle O. Computational analysis of cell-to-cell heterogeneity in single-cell RNA-sequencing data reveals hidden subpopulations of cells. Nat Biotechnol. 2015;33(2):155-60. Epub 2015/01/20. doi: 10.1038/nbt.3102. PubMed PMID: 25599176.
21. Farber DL, Yudanin NA, Restifo NP. Human memory T cells: generation, compartmentalization and homeostasis. Nat Rev Immunol. 2014;14(1):24-35. Epub 2013/12/18. doi: 10.1038/nri3567. PubMed PMID: 24336101; PMCID: PMC4032067.
22. Mahnke YD, Brodie TM, Sallusto F, Roederer M, Lugli E. The who's who of T-cell differentiation: human memory T-cell subsets. Eur J Immunol. 2013;43(11):2797-809. Epub 2013/11/22. doi: 10.1002/eji.201343751. PubMed PMID: 24258910.
23. Kern F, Khatamzas E, Surel I, Frommel C, Reinke P, Waldrop SL, Picker LJ, Volk HD. Distribution of human CMV-specific memory T cells among the CD8pos. subsets defined by CD57, CD27, and CD45 isoforms. Eur J Immunol. 1999;29(9):2908-15. Epub 1999/10/03. doi: 10.1002/(SICI)1521-4141(199909)29:09<2908::AID-IMMU2908>3.0.CO;2-8. PubMed PMID: 10508265.
24. Brenchley JM, Karandikar NJ, Betts MR, Ambrozak DR, Hill BJ, Crotty LE, Casazza JP, Kuruppu J, Migueles SA, Connors M, Roederer M, Douek DC, Koup RA. Expression of CD57 defines replicative senescence and antigen-induced apoptotic death of CD8+ T cells. Blood. 2003;101(7):2711-20. Epub 2002/11/16. doi: 10.1182/blood-2002-07-2103. PubMed PMID: 12433688.
25. Teo SM, Mok D, Pham K, Kusel M, Serralha M, Troy N, Holt BJ, Hales BJ, Walker ML, Hollams E, Bochkov YA, Grindle K, Johnston SL, Gern JE, Sly PD, Holt PG, Holt KE, Inouye M. The infant nasopharyngeal microbiome impacts severity of lower respiratory infection and risk of asthma development. Cell Host Microbe. 2015;17(5):704-15. Epub 2015/04/14. doi: 10.1016/j.chom.2015.03.008. PubMed PMID: 25865368; PMCID: PMC4433433.
26. Harimaya A, Takada R, Hendolin PH, Fujii N, Ylikoski J, Himi T. High incidence of Alloiococcus otitidis in children with otitis media, despite treatment with antibiotics. J Clin Microbiol. 2006;44(3):946-9. Epub 2006/03/07. doi: 10.1128/JCM.44.3.946-949.2006. PubMed PMID: 16517881; PMCID: PMC1393137.
27. Lemanske RF, Jr. The childhood origins of asthma (COAST) study. Pediatr Allergy Immunol. 2002;13(s15):38-43. Epub 2003/04/12. PubMed PMID: 12688623.
28. Muench MO, Pott Bartsch EM, Chen JC, Lopoo JB, Barcena A. Ontogenic changes in CD95 expression on human leukocytes: prevalence of T-cells expressing activation markers and identification of CD95-CD45RO+ T-cells in the fetus. Dev Comp Immunol. 2003;27(10):899-914. Epub 2003/07/26. doi: S0145305X03000818 [pii]. PubMed PMID: 12880639.
29. Tezuka T, Sugita K, Mizobe N, Goi K, Miyamoto N, Nakamura M, Kagami K, Yokoyama T, Nakazawa S. Transient increase in CD45RO expression on T lymphocytes in infected newborns. Pediatr Res. 1998;43(2):283-90. Epub 1998/02/25. PubMed PMID: 9475298.
30. Mold JE, Venkatasubrahmanyam S, Burt TD, Michaelsson J, Rivera JM, Galkina SA, Weinberg K, Stoddart CA, McCune JM. Fetal and adult hematopoietic stem cells give rise to distinct T cell lineages in humans. Science. 2010;330(6011):1695-9. doi: 10.1126/science.1196509. PubMed PMID: 21164017; PMCID: 3276679.
31. Michaelsson J, Mold JE, McCune JM, Nixon DF. Regulation of T cell responses in the developing human fetus. J Immunol. 2006;176(10):5741-8. PubMed PMID: 16670279.
32. Zhivaki D, Lo-Man R. In utero development of memory T cells. Semin Immunopathol. 2017;39(6):585-92. Epub 2017/09/14. doi: 10.1007/s00281-017-0650-0. PubMed PMID: 28900758.
33. Sprent J, Surh CD. Normal T cell homeostasis: the conversion of naive cells into memory-phenotype cells. Nat Immunol. 2011;12(6):478-84. Epub 2011/07/09. PubMed PMID: 21739670; PMCID: PMC3434123.

34. Byrne JA, Stankovic AK, Cooper MD. A novel subpopulation of primed T cells in the human fetus. J Immunol. 1994;152(6):3098-106. Epub 1994/03/15. PubMed PMID: 8144905.
35. Madan JC, Koestler DC, Stanton BA, Davidson L, Moulton LA, Housman ML, Moore JH, Guill MF, Morrison HG, Sogin ML, Hampton TH, Karagas MR, Palumbo PE, Foster JA, Hibberd PL, O'Toole GA. Serial analysis of the gut and respiratory microbiome in cystic fibrosis in infancy: interaction between intestinal and respiratory tracts and impact of nutritional exposures. MBio. 2012;3(4). Epub 2012/08/23. doi: 10.1128/mBio.00251-12. PubMed PMID: 22911969; PMCID: PMC3428694.
36. Marsland BJ, Trompette A, Gollwitzer ES. The Gut-Lung Axis in Respiratory Disease. Ann Am Thorac Soc. 2015;12 Suppl 2:S150-6. Epub 2015/11/26. doi: 10.1513/AnnalsATS.201503-133AW. PubMed PMID: 26595731.
37. Harris PA, Taylor R, Minor BL, Elliott V, Fernandez M, O'Neal L, McLeod L, Delacqua G, Delacqua F, Kirby J, Duda SN, Consortium RE. The REDCap consortium: Building an international community of software platform partners. J Biomed Inform. 2019;95:103208. Epub 2019/05/13. doi: 10.1016/j.jbi.2019.103208. PubMed PMID: 31078660.
38. Harris PA, Taylor R, Thielke R, Payne J, Gonzalez N, Conde JG. Research electronic data capture (REDCap)--a metadata-driven methodology and workflow process for providing translational research informatics support. J Biomed Inform. 2009;42(2):377-81. Epub 2008/10/22. doi: 10.1016/j.jbi.2008.08.010. PubMed PMID: 18929686; PMCID: PMC2700030.
39. Nelson EK, Piehler B, Eckels J, Rauch A, Bellew M, Hussey P, Ramsay S, Nathe C, Lum K, Krouse K, Stearns D, Connolly B, Skillman T, Igra M. LabKey Server: an open source platform for scientific data integration, analysis and collaboration. BMC bioinformatics. 2011;12:71. doi: 10.1186/1471-2105-12-71. PubMed PMID: 21385461; PMCID: 3062597.
40. Scheible K, Secor-Socha S, Wightman T, Wang H, Mariani TJ, Topham DJ, Pryhuber G, Quataert S. Stability of T cell phenotype and functional assays following heparinized umbilical cord blood collection. Cytometry A. 2012;81(11):937-49. Epub 2012/10/03. doi: 10.1002/cyto.a.22203. PubMed PMID: 23027690; PMCID: PMC4029066.
41. Hahne F, LeMeur N, Brinkman RR, Ellis B, Haaland P, Sarkar D, Spidlen J, Strain E, Gentleman R. flowCore: a Bioconductor package for high throughput flow cytometry. BMC bioinformatics. 2009;10:106. Epub 2009/04/11. doi: 10.1186/1471-2105-10-106. PubMed PMID: 19358741; PMCID: PMC2684747.
42. Hahne FG, N.; Khodabakhshi, AH.; Wong, C.; Lee, K. . flowStats: Statistical methods for the analysis of flow cytometry data. 3.40.1 ed2019.
43. Fadrosh DW, Ma B, Gajer P, Sengamalay N, Ott S, Brotman RM, Ravel J. An improved dual-indexing approach for multiplexed 16S rRNA gene sequencing on the Illumina MiSeq platform. Microbiome. 2014;2(1):6. Epub 2014/02/25. doi: 10.1186/2049-2618-2-6. PubMed PMID: 24558975; PMCID: PMC3940169.
44. Caporaso JG, Kuczynski J, Stombaugh J, Bittinger K, Bushman FD, Costello EK, Fierer N, Pena AG, Goodrich JK, Gordon JI, Huttley GA, Kelley ST, Knights D, Koenig JE, Ley RE, Lozupone CA, McDonald D, Muegge BD, Pirrung M, Reeder J, Sevinsky JR, Turnbaugh PJ, Walters WA, Widmann J, Yatsunenko T, Zaneveld J, Knight R. QIIME allows analysis of high-throughput community sequencing data. Nat Methods. 2010;7(5):335-6. Epub 2010/04/13. doi: 10.1038/nmeth.f.303. PubMed PMID: 20383131; PMCID: PMC3156573.
45. Bolyen E. QIIME 2: Reproducible, interactive, scalable, and extensible microbiome data science. PeerJ Preprints. 2018;e27285v1.
46. Callahan BJ, McMurdie PJ, Rosen MJ, Han AW, Johnson AJ, Holmes SP. DADA2: High-resolution sample inference from Illumina amplicon data. Nat Methods. 2016;13(7):581-3. Epub 2016/05/24. doi: 10.1038/nmeth.3869. PubMed PMID: 27214047; PMCID: PMC4927377.
47. DeSantis TZ, Hugenholtz P, Larsen N, Rojas M, Brodie EL, Keller K, Huber T, Dalevi D, Hu P, Andersen GL. Greengenes, a chimera-checked 16S rRNA gene database and workbench compatible with ARB. Appl Environ Microbiol. 2006;72(7):5069-72. Epub 2006/07/06. doi: 10.1128/AEM.03006-05. PubMed PMID: 16820507; PMCID: PMC1489311.
48. Katoh K, Standley DM. MAFFT multiple sequence alignment software version 7: improvements in performance and usability. Mol Biol Evol. 2013;30(4):772-80. Epub 2013/01/19. doi: 10.1093/molbev/mst010. PubMed PMID: 23329690; PMCID: PMC3603318.
49. Price MN, Dehal PS, Arkin AP. FastTree 2--approximately maximum-likelihood trees for large alignments. PLoS One. 2010;5(3):e9490. Epub 2010/03/13. doi: 10.1371/journal.pone.0009490. PubMed PMID: 20224823; PMCID: PMC2835736.

50. Lozupone C, Lladser ME, Knights D, Stombaugh J, Knight R. UniFrac: an effective distance metric for microbial community comparison. ISME J. 2011;5(2):169-72. Epub 2010/09/10. doi: 10.1038/ismej.2010.133. PubMed PMID: 20827291; PMCID: PMC3105689.
51. Holmes I, Harris K, Quince C. Dirichlet multinomial mixtures: generative models for microbial metagenomics. PLoS One. 2012;7(2):e30126. Epub 2012/02/10. doi: 10.1371/journal.pone.0030126. PubMed PMID: 22319561; PMCID: PMC3272020.
52. Morgan M. DirichletMultinomial: Dirichlet-Multinomial Mixture Model Machine Learning for Microbiome Data. R package version. 2019;1.22.0.
53. Team RC. R: A language and environment for statistical computing. . R Foundation for Statistical Computing, Vienna, Australia. 2013.
54. Anderson-Bergman C. icenReg: Regression models for interval censored data in R. Journal of Statistical Software. 2017;81(12):1-23.
55. Halekoh UH, S; Yan, J. The R package geepack for generalized estimating equations. Journal of Statistical Software 2006;15(2):1-11.
56. Bates DM, M; Bolker, B; Walker, S. Fitting Linear Mixed-Effects Models Using lme4. Journal of Statistical Software. 2015;67(1):1-48.
57. Friedman JH, T.; Tibshirani, R. Regularization Paths for Generalized Linear Models via Coordinate Descent. J Statistical Software. 2010;33(1).
58. Bischl BL, M.; Kotthoff, L.; Schiffner, J.; Richter, J.; Studerus, E.; Casalicchio, G.; Jones, Z. mlr: Machine Learning in R. J Machine Learning Research 1. 2000:1-48.

TPHE	subjects	samples
3 timepoints	78	234
2 timepoints	82	164
1 timepoint	16	16
total	**176**	**414**

TPHE	samples	pre-term	full-term
birth	147	65	82
discharge	163	87	76
12-month	104	58	46
total	**414**	*210*	*204*

ICS	subjects	samples
3 timepoints	69	207
2 timepoints	89	178
1 timepoint	19	19
total	**177**	**404**

ICS	samples	pre-term	full-term
birth	147	64	83
discharge	155	84	71
12-month	102	55	47
total	**404**	*203*	*201*

TPHE_ICS	subjects	samples
3 timepoints	67	201
2 timepoints	83	166
1 timepoint	18	18
total	**168**	**385**

TPHE_ICS	samples	pre-term	full-term
birth	141	63	78
discharge	150	81	69
12-month	94	51	43
total	**385**	*195*	*190*

Supplementary Table 1: Subject numbers for immunophenotyping

Figure Description	Site	Samples	Subjects
Microbiome CGA & CST PCoA plots	Both NAS	1748	149
	Both REC	1899	143
Microbiome CST Occurrence Over CGA	NAS	1748	149
	REC	1899	143
Microbiome Composition Heatmaps	NAS	1748	149
	REC	1899	143
Immuno IST Composition Heatmaps	TPHE	414	176
	ICS	404	177
Immuno IST Occurrence Over CGA	TPHE	414	176
	ICS	404	177
Immuno IST Avg. Occurrence GAB/CGA	TPHE	414	176
	ICS	404	177
NAS 8 Occurrence vs TPHE ISTs	Birth	68	68
	Discharge	95	95
CST-Immuno Association Networks	NAS	1589	109
	REC	1697	117

Supplementary Table 2: Subject numbers microbiome and combined analyses

Cytometer: BDLSRII (URMC FlowCore - Animal)

Tphe Functional Panel (RPRC 12-0012)

Laser	Long Pass	Band Pass	PMT	Detector	Marker	Color	Clone	Company	Catalog #
488	505	515/20	BB	B515	**CD122**	BB 515	Mik-β	BD Biosciences	564688
488	685	710/50	BA	B710	**Perforin**	PerCP-Cy5.5	dG9	Biolegend	308114
407		450/50	VH	V450	**Granzyme B**	BV 421	GB11	BD Biosciences	563389
407	535	550/40	VG	V550	**Live/Dead**	Aqua		Life Technologies	L34957
407	570	585/42	VE	V585	**CD3**	BV 570	UCHT1	Biolegend	300436
407	595	605/40	VD	V605	**CD31**	BV 605	WM59	BD Biosciences	562855
407	630	660/40	VC	V660	**CD127**	BV 650	HIL-7R-M21	BD Biosciences	563225
407	670	705/70	VB	V705	**CD45RO**	BV 711	UCHL1	BD Biosciences	563722
407	740	780/60	VA	V780	**CD8a**	BV 785	RPA-T8	Biolegend	301045
633		660/20	RC	R660	**KLRG1**	APC	13F12F2	eBioscience	17-9488-42
633	685	710/50	RB	R710	**CD185 (CXCR**	APC-R700	RF8B2	BD Biosciences	565191
633	740	780/60	RA	R780	**CD197 (CCR7**	APC-Cy7	G043H7	Biolegend	353212
532		575/24	GE	G575	**Foxp3**	PE	236A/E7	eBioscience	12-4777-42
532	600	610/20	GD	G610	**CD4**	PE-TR	S3.5	Invitrogen	MHCD0417
532	640	660/40	GC	G660	**CD28**	PE-Cy5	CD28.2	BD Biosciences	561791
532	740	780/40	GA	G780	**CD57**	PE-Cy7	TB01	eBioscience	25-0577-42

ICS Functional Panel (RPRC 12-0012)

Cytometer: BDLSRII (URMC FlowCore - Animal)

Laser	Long Pass	Band Pass	PMT	Detector	Marker	Color	Clone	Company	Catalog #
488	505	515/20	BB	B515	**IL-8**	FITC	E8N1	BioLegend	511406
407		450/50	VH	V450	**IL-17**	Pacific Blue	BL168	BioLegend	512312
407	535	550/40	VG	V550	**Live/Dead**	Aqua	polyclonal	Life Technologies	L34957
407					**CD14**	BV510	MϕP9	BD Biosciences	563079
407	570	585/42	VE	V585	**CD8a**	BV570	RPA-T8	BioLegend	301037
407	595	605/40	VD	V605	**IL-2**	BV605	MQ1-17H12	BD Biosciences	564165
407	630	660/40	VC	V660	**CD45RA**	BV650	HI100	BD Biosciences	563963
407	670	705/70	VB	V705	**IL-10**	BV711	JES3-9D7	BD Biosciences	564050
407	740	780/60	VA	V780	**TNFa**	BV785	MAb11	BioLegend	502948
633		660/20	RC	R660	**IL-6**	APC	MQ2-13A5	BD Biosciences	561441
633	685	710/50	RB	R710	**CD3**	AF700	UCHT1	BD Biosciences	557943
633	740	780/60	RA	R780	**CD69**	APC-Cy7	FN50	BioLegend	310914
532		575/24	GE	G575	**IL-4**	PE	MP4-25D2		
532	600	610/20	GD	G610	**CD107a**	PE-CF594	H4A3	BD Biosciences	562628
532	690	710/50	GB	G710	**CD4**	PE-Cy5.5	S3.5	ThermoFischer	MHCD0418
532	740	780/40	GA	G780	**IFN-g**	PE-Cy7	B27	BD Biosciences	557643

Supplementary fig 1. Flow cytometry channels and antibodies for ICS and Tphe panels.

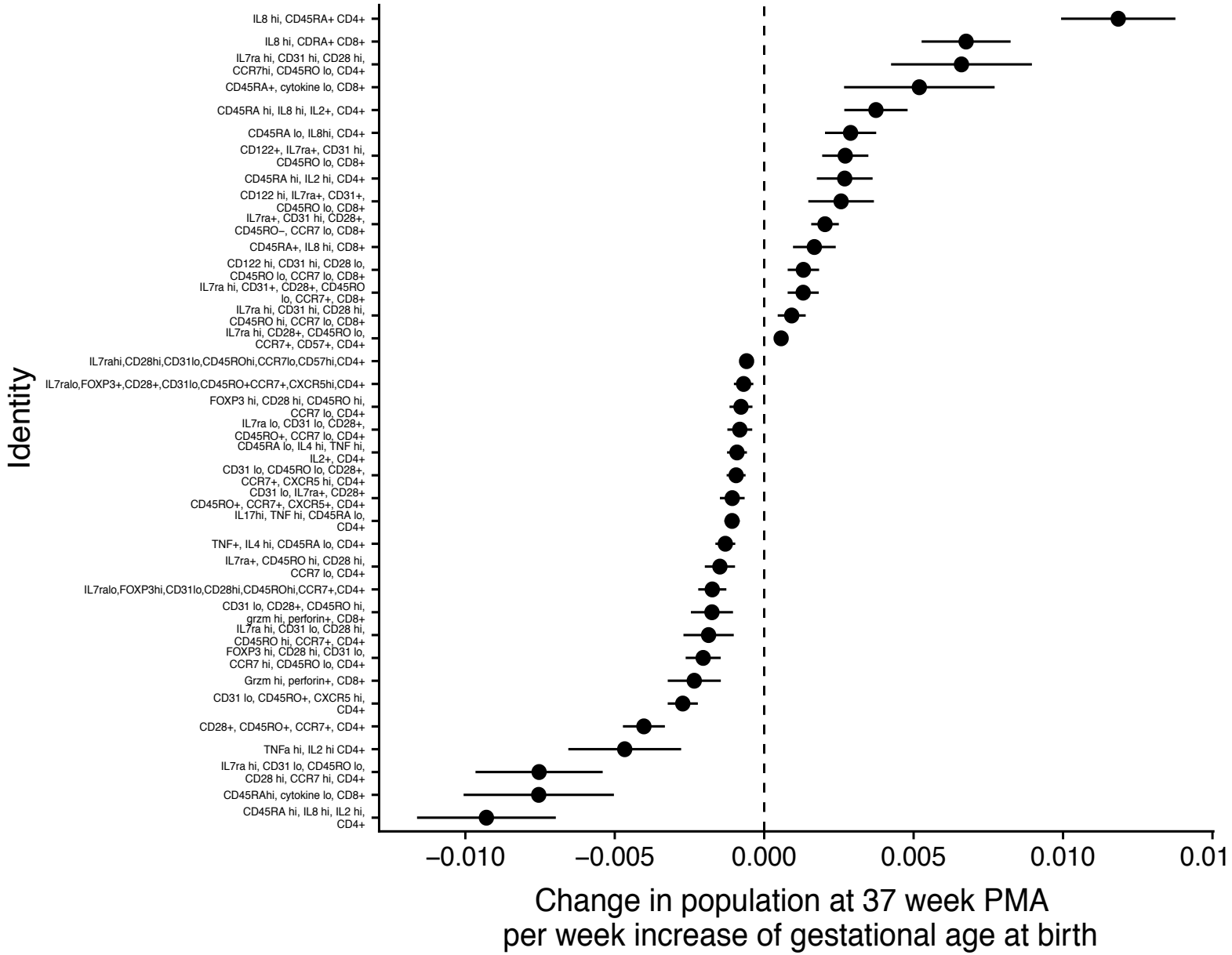

Supplementary fig 2. Estimated change in metacluster abundance at 37 weeks PMA per week increase gestational age at birth.

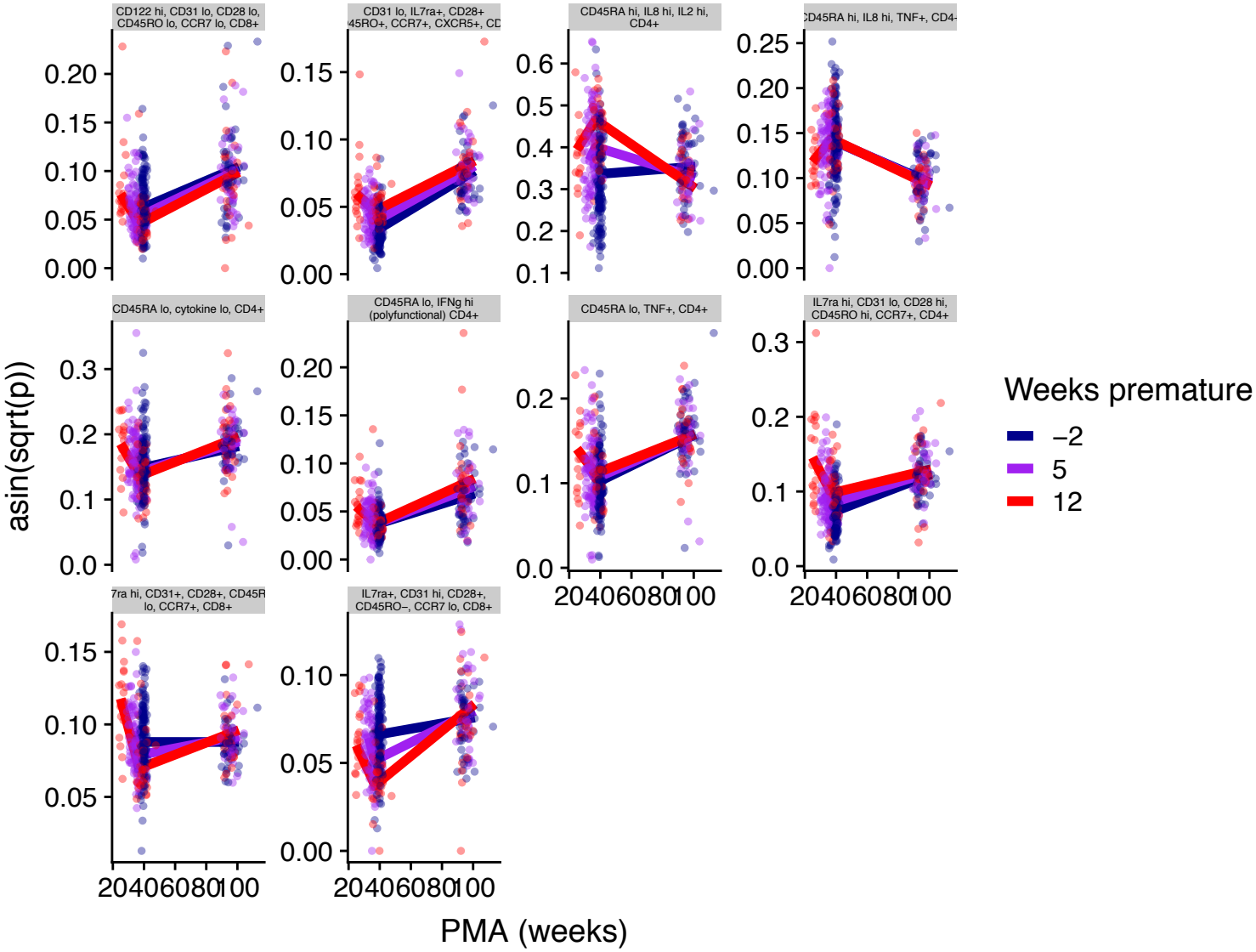

Supplementary fig 3. Meta clusters with non-monotone trajectories as a function of PMA.

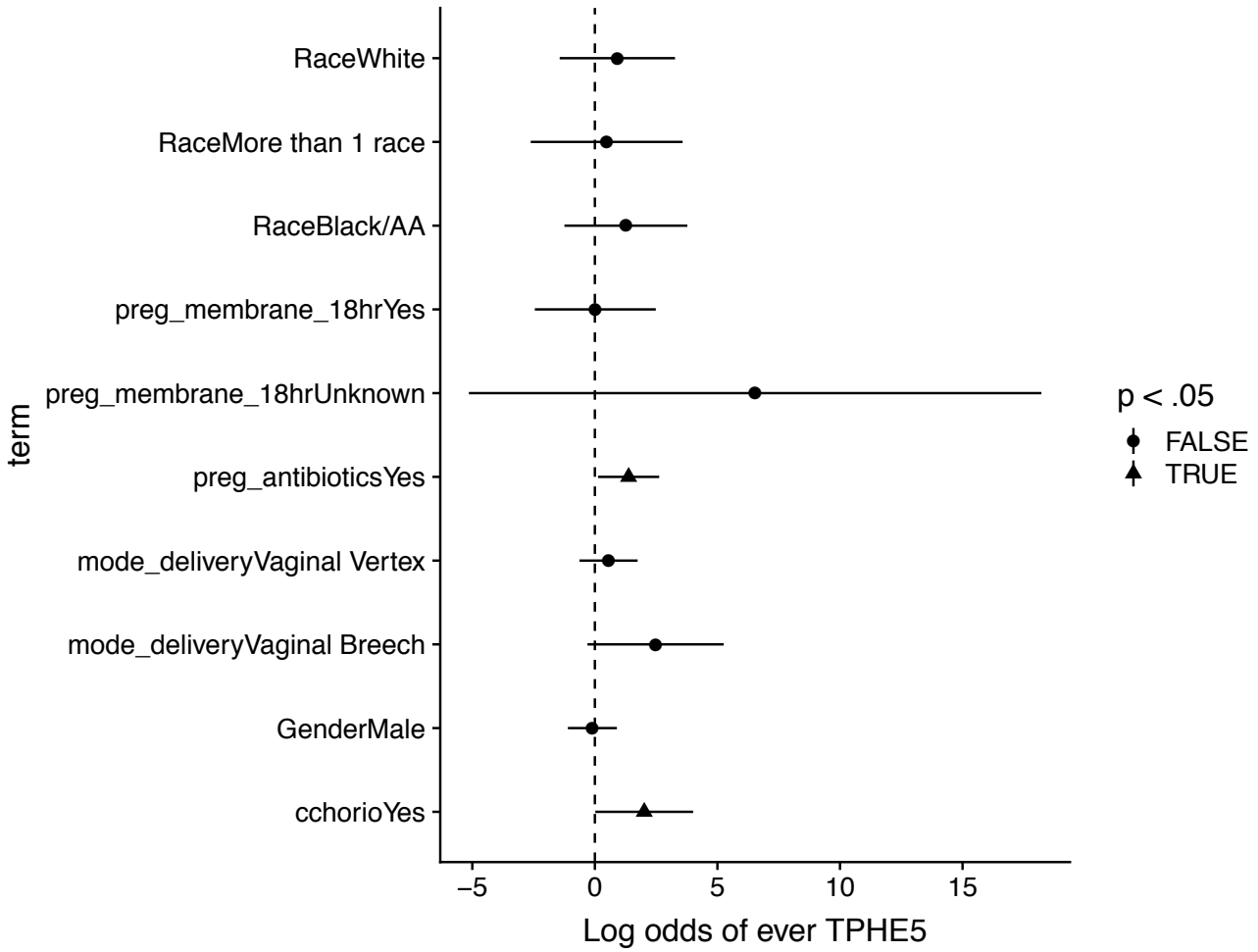

Supplementary fig 4. Risk factors for subjects ever entering IST Tphe5. A joint logistic regression of the form Tphe5 ~ s(gestation_age_birth)+ race + preg_membrane + preg_antibiotics + mode_delivery + gender + cchorio was run using R package mgcv version 1.8.24. The term s(gestational_age_birth) represents an arbitrary, smooth function of gestational age at birth that was simultaneously estimated with the other parametric model terms.

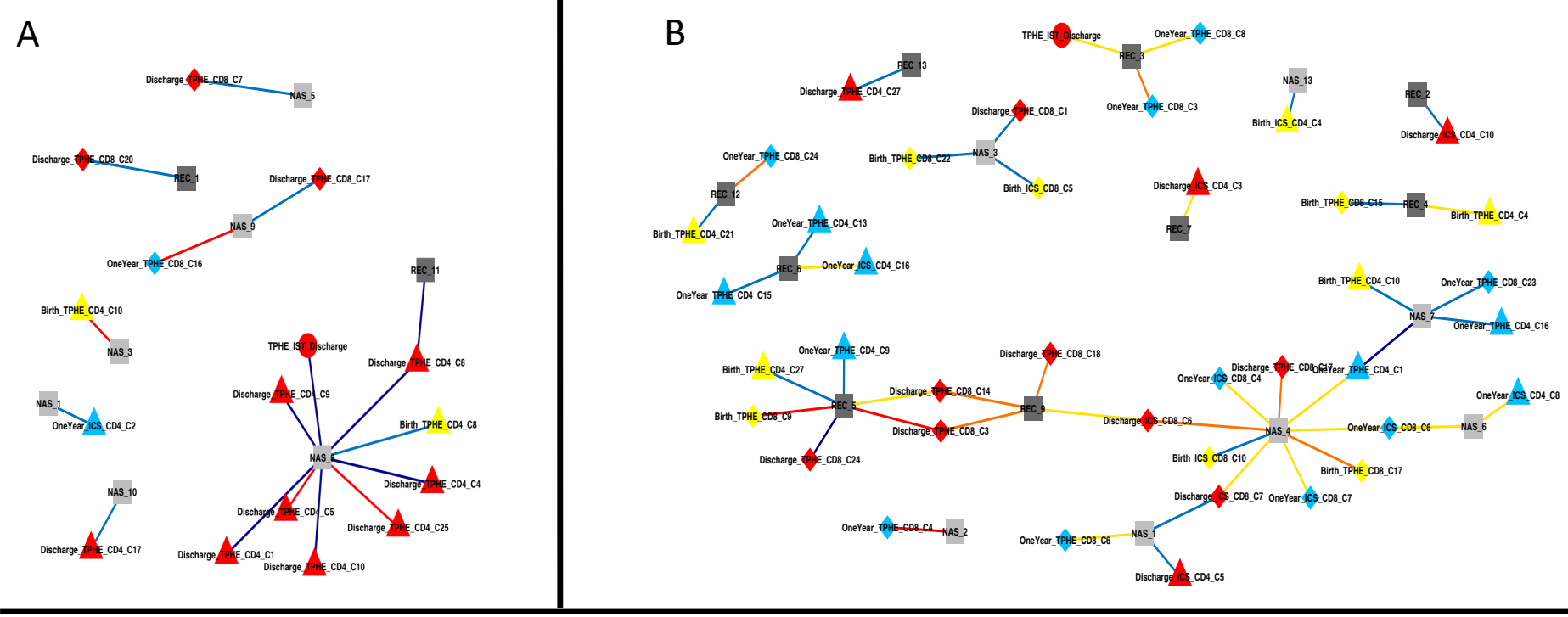

Supplemental fig 5. Networks of associations between CST occurrence and T cell populations and ISTs. (A) Logistic regression was used to assess the relationship between T cell populations or ISTs at birth, discharge, or one year and the probability of ever observing a given CST within a subject. (B) Interval censored survival modeling was used to assess the relationship between T cell populations and ISTs at birth, discharge, or one year and the time to occurrence of a given CST within a subject. Mode of delivery and gestational age at birth were included as covariates in both types of models. All significant associations (after multiple test correction) are plotted, with edges between an immunological parameter and a CST indicating a significant relationship. Edges are colored according to the direction of the relationship and the magnitude of its significance. Nodes are colored to indicate time point or body site and are shaped to distinguish between CSTs, ISTs, and individual T cell populations.

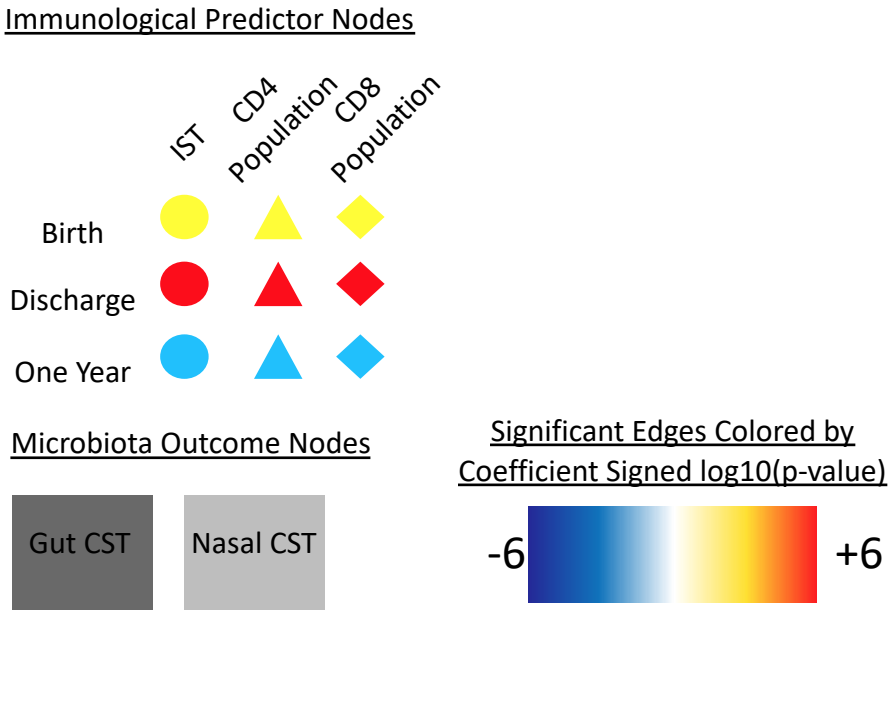

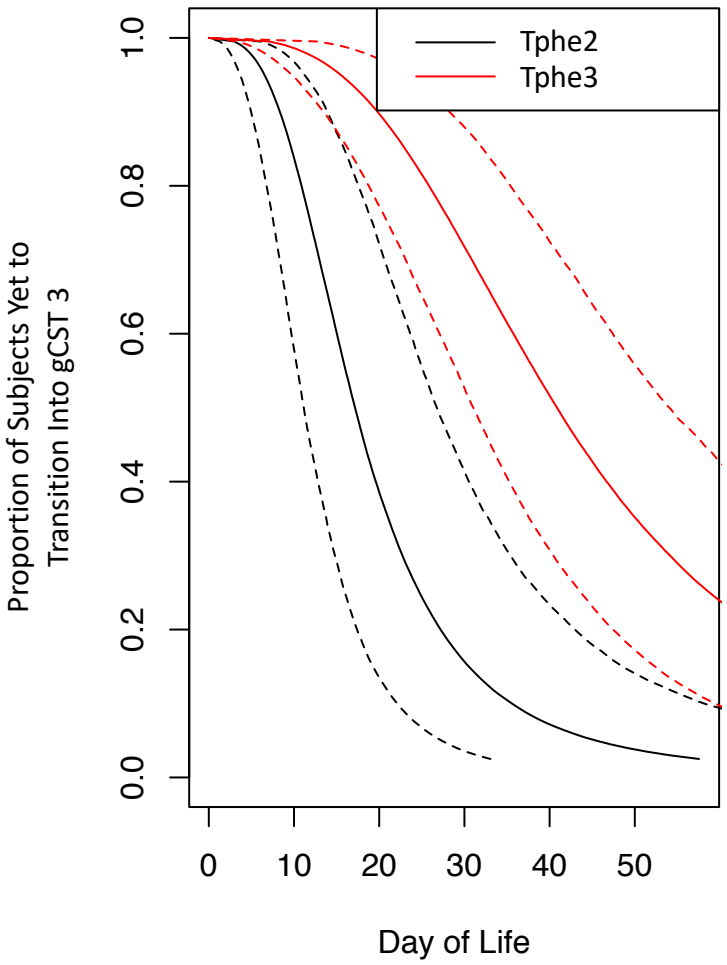

Supplemental fig 6. Time to transition into gCST 3 based on Tphe IST at discharge. Survival analysis using an accelerated failure time model was used to assess the time to initially transition into gCST 3 as a function of Tphe IST at discharge, gestational age at birth, and mode of delivery. Fitted mean probabilities of not having transitioned in gCST 3 are shown for infants born at 30 weeks GA by Cesarean section, with 95% confidence intervals. Tphe3 at discharge significantly delayed initial transition into gCST 3.

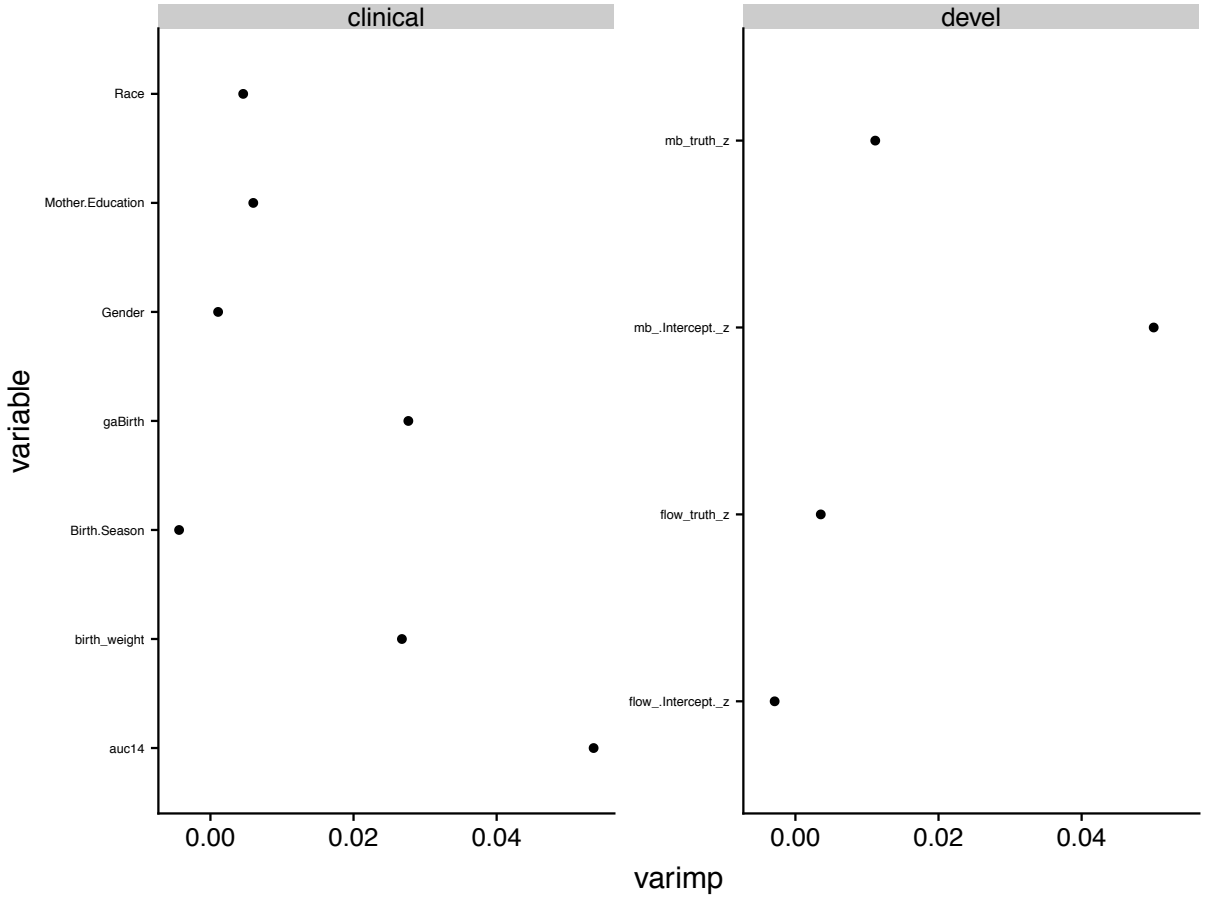

Supplementary figure 7. Random forest variable importance plots for clinical and developmental index models. Larger values represent greater decreases in the Gini purity coefficient. Importance was calculated using the default method in R package randomForestSRC version 2.7.0.